Title
PION PRODUCTION NEAR MID-RAPIDITY IN HIGH ENERGY HEAVY ION COLLISIONS

Author
Frankel, K.A.

Publication Date
1985-04-01

Lawrence Berkeley Laboratory
UNIVERSITY OF CALIFORNIA

Submitted to The Physical Review, C

PION PRODUCTION NEAR MID-RAPIDITY
IN HIGH ENERGY HEAVY ION COLLISIONS

K.A. Frankel, J.A. Bistirlich, R. Bossingham,
H.R. Bowman, K.M. Crowe, C.J. Martoff, D.L. Murphy,
J.O. Rasmussen, J.P. Sullivan, E. Yoo, W.A. Zajc,
J.P. Miller, O. Hashimoto, M. Koike, J. Péter,
W. Benenson, G.M. Crawley, E. Kashy,
J.A. Nolen, Jr., and J. Quebert

April 1985

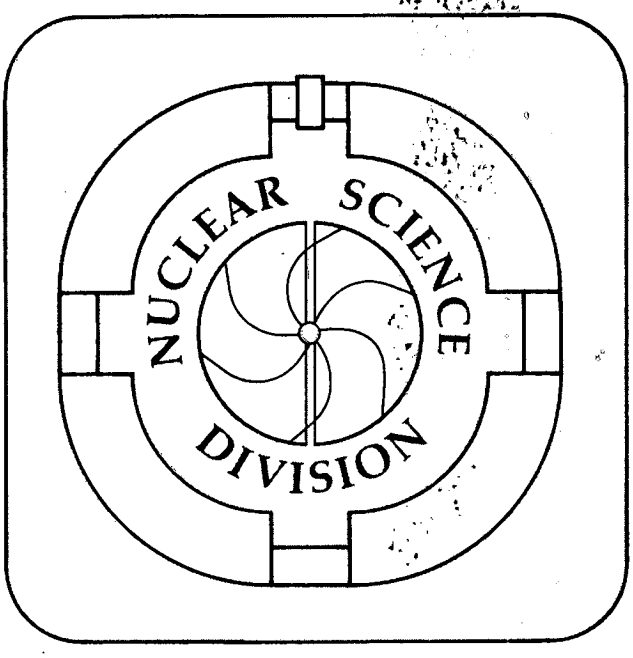

Prepared for the U.S. Department of Energy under Contract DE-AC03-76SF00098

DISCLAIMER

PION PRODUCTION NEAR MID-RAPIDITY IN HIGH ENERGY HEAVY ION COLLISIONS

K.A. Frankel, J.A. Bistirlich, R. Bossingham, H.R. Bowman, K.M. Crowe, C.J. Martoff,* D. L. Murphy, J.O. Rasmussen, J.P. Sullivan,** E. Yoo, and W.A. Zajc†
Nuclear Science Division; Lawrence Berkeley Laboratory
University of California, Berkeley CA 94720

and

J.P. Miller
Department of Physics, Boston University
Boston, MA 02215

and

O. Hashimoto and M. Koike
Institute for Nuclear Study, University of Tokyo, Tokyo, Japan, and
Lawrence Berkeley Laboratory, Berkeley, CA 94720

and

J. Péter††
Institut de Physique Nucléaire, Orsay, France

and

W.Benenson, G.M. Crawley, E. Kashy, and J.A. Nolen, Jr.
Michigan State University, East Lansing, MI 48824

and

J. Quebert
Universite de Bordeaux, Le Haut-Vigneau, 33170, Gradignan, France

*Present address: Department of Physics, Stanford University, Stanford, CA 94305

**Present address: Cyclotron Institute, Texas A&M University, College Station, Texas 77843

†Present address: Physics Department, University of Pennsylvania, Philadelphia, Pennsylvania

††Present address: GANIL, Caen, France

April 8, 1985

Abstract: Doubly differential cross sections for producing π^+ and π^- were measured for several target-projectile combinations. They were ^{40}Ar + C, Ca, and U at 1050 A MeV and ^{20}Ne + Be and NaF at 655 A MeV. The π^-/π^+ ratios are smaller than those expected from several Coulomb effect calculations. The Ne + NaF $\rightarrow \pi^-$ data exhibit a peak at 90° in the center of mass and $p_\pi = 0.4 m_\pi c$.

PACS numbers: 25.70.-z

I. Introduction

Pion production at low momentum in the center of mass ($p_\pi < m_\pi c$) in relativistic heavy ion collisions has been extensively studied recently. Enhancements of the pion yield at the rapidity of center of mass (i.e., mid-rapidity) have been observed[1-3], where rapidity y = (1/2) $\ln[(E + p_\parallel)/(E - p_\parallel)]$. This enhancement is evident when the heavy-ion data are compared to the 730 MeV p + p $\rightarrow \pi^+$ yields,[4] which show a minimum in the angular distribution at 90° in the center-of-mass for low p_π. When the contours of invariant differential cross section are plotted, these enhancements appear as plateaus. For the reaction 800A MeV Ne + NaF $\rightarrow \pi^+$, Chiba et al.[2] observed a peak at the center-of-mass rapidity at $p_\perp \simeq 0.5\ m_\pi c$. The height of the peak was about 1.4 times the smoothly varying component of the cross-section (which will be referred to as the "background"). The peak was also observed by Chibu et al.[2] when heavier targets were used. In a similar experiment with 1.05A GeV ^{40}Ar + Ca $\rightarrow \pi^+$, Wolf et al.[1] observed a peak at $p_\perp \simeq 0.4\ m_\pi c$ which had a height ~1.3 times the "background." The peak is enhanced by selecting pions from events of high total multiplicity.[1] In an experiment at lower energy, 400 A MeV ^{20}Ne + NaF (and heavier targets) $\rightarrow \pi^+$, Nakai et al.[5] did not observe a mid-rapidity enhancement.

Numerous explanations for these low energy π^+ peaks or ridges have been suggested:

1) Collective flow effects, such as hydrodynamic "splashing" or "jetting" in the perpendicular direction, might enhance pion spectra

at the collective velocity[1].

2) Shadowing(absorption) effects from spectator material, which should be strongest for pions moving near the Δ (3,3) resonance in the spectator frame, could selectively absorb pions and create valleys around the low energy "bump."[5,6]

3) In certain spin-isospin states two deltas are presumed to strongly bind. The pionic decay of such "di-deltas" would give a low energy pion component.[5]

4) Monte-Carlo cascade calculations by Yariv and Fraenkel[7] show a mid-rapidity bump, though at somewhat higher $p_\perp$ than experimentally observed. They offer no detailed explanations of its origin.

5) Several authors have studied the possibility that the low energy π^+ bumps could be primarily due to simple Coulomb effects.[8-10] Coulomb effects on pion spectra have been clearly established,[8-14] but we believe that the π^- evidence we present here rules out the simple Coulomb explanation for low energy pion bumps in the mid-rapidity region.

6) Pion orbiting, probably enhanced by boson properties of pions, constitutes one of the most interesting explanations, particularly since it relates the observed pion momentum of 0.4-0.5 $m_\pi c$ to a nuclear size of approximately 3fm by the uncertainty relation $R \sim \hbar/p$ (i.e., Fourier transform). For discussions of the boson condensation aspects see references 15 and 16. For hadronic pionic binding aspects see references 17-19.

We have extended the pion measurements by obtaining inclusive spectra for both π^- and π^+ production. Some of these results have been reported previously[3] and are included here for completeness. By measuring both π^- and π^+ spectra we are better able to distinguish the role of Coulomb effects in the observed pion spectra. We note that if one hopes to obtain detailed information on the structure of the mid-rapidity cross section it is necessary to have excellent momentum and angular resolution typically ($\Delta p/p < 5\%$, $\Delta\theta < 4°$), and small statistical uncertainties (less than 5%). In contrast to the peaks observed at beam velocity,[12] where the enhancement has been observed to be a factor as large as 10 (e.g. 281A MeV ^{20}Ne + NaF $\rightarrow \pi^-$), the observed enhancement at mid-rapidity is only about 30-40%, so careful work is necessary to observe it.

II. Description of Experiment

The reactions of 1.05A GeV ^{40}Ar with C, Ca, and U targets and of 655A MeV ^{20}Ne with Be and NaF targets were studied. Data for both positive and negative pions were collected for each projectile-target combination. The data were taken with a magnetic spectrometer at the Lawrence Berkeley Laboratory BEVALAC. Because the apparatus has been described elsewhere[13], only a brief description is given here. Particles emerging from the target were bent ~180° in the magnet and passed through two multi-wire proportional counters (MWPC's), which were used to define their trajectories. The particles were then stopped in an eleven-element scintillator range stack. From their

radii of curvature in the magnetic field, the momenta of the particles were determined. Using the momentum, the energy losses in the first two scintillators (ΔE's), and the range of the particles, pions could be very clearly distinguished from other particles. Data for the ^{40}Ar experiment were taken with the spectrometer rotated 15° from the 0° position shown in Fig. 1. This centers the acceptance at a laboratory angle of 15° (the "central angle" in Table 1). The 655A MeV Ne data were taken with the spectrometer in the 0° position except for some of the $^{20}Ne + NaF \rightarrow \pi^-$ data. In this case data were taken at 0° and at 30°. The beams, targets, and spectrometer angles used to obtain the results reported here are summarized in Table 1.

III. Results

The doubly differential invariant cross sections are plotted in various forms in Figures 2-11. Figures 2-4 are plots of invariant cross section ($Ed^3\sigma/dp^3$) vs. momentum for the C, Ca, and U targets. Data at 15° for 1.05 A GeV ^{40}Ar + C, Ca, U are shown in Fig. 5. Figures 6 and 7 present the data for the Ne + NaF and Ne + Be experiments. Isometric plots of $Ne + NaF \rightarrow \pi^-$ and π^+ are shown in Figs. 8 and 9. Figure 10 shows cuts at 0° and at $y = y_{CM}$ (90° CM) for the $Ar + Ca \rightarrow \pi^+$ and π^- data. Figure 11 shows cuts at 0° and 90° for the $Ne + NaF \rightarrow \pi^+$ and π^- data. In Figure 11 the solid line is inferred from π^+ data of Nagamiya et al.;[20] we have interpolated in beam energy between results at 400 A MeV and 800 A MeV results and have extrapolated from Nagamiya's higher momentum data, the lowest

point of which would be on the right-hand border of our Figure 11b. The data for the reactions are listed in Tables II—XI in LBL Report No. 16000, available on request from the Report Librarian, Nuclear Science Division, Lawrence Berkeley Laboratory, Berkeley, CA 94720.

IV. Discussion

The Ar + Ca → π^+ data are quite flat in the region that we measured. Although there is some disagreement between our data and some data points of Wolf et al.[1] reflected through the center-of-mass, we believe that the differences are explainable by a combination of statistics and resolution of both experiments (see plots and discussion in our Ref. 3). We have excellent agreement where the data are directly comparable; there are differences only when comparing data reflected about the center-of-mass, a comparison which is only approximately correct, as our systems are not truly symmetric. The beam velocity π^- enhancements and π^+ depressions are clearly observable in the 655 A MeV ^{20}Ne + NaF and Be data (see Figs. 6 and 7).

Surprisingly, we find a broad maximum around $y_{CM} = 0$, $p_\perp = 0.4\ m_\pi c$ in the Ne + NaF → π^- data (Fig. 11). The invariant cross section at the peak is 3 b/sr^{-1} GeV^{-2} c, while at $y_{CM} = 0$, $p_\perp = 0$ it is 2.4, so the peak is only about 25% above "background." Unfortunately there was no time available to take data for laboratory angles greater than 20° for the π^+, so we were unable to determine if there is also a peak for π^+ in the same place for this system, but

similar peaks have already been observed in π^+ spectra.[1,2]

Since low energy pion bumps have been observed in π^+ by Chiba et al.[2] and Wolf et al.,[1] and are now observed for the first time in π^- data, we believe that the peaks cannot be due solely to Coulomb effects. This is further apparent when we examine the π^-/π^+ ratios. The ratios at the nucleon-nucleon center-of-mass are summarized in Table I. For the 1.05 A GeV Ar + Ca case the ratio is 1.5 ± 0.2. Theoretical predictions by Cugnon and Koonin[9] give a prediction of 5.5, and the formulas of Gyulassy and Kauffmann[10] predict a ratio of 2.7, which are much higher than shown by the data. These predictions are based on the assumption that the pions travel on trajectories which are under the influence only of Coulomb forces when passing near and through the projectile and target spectators and the expanding fireball. Ratios for the heavier targets are also below the theoretical expectations.

The large discrepancy between the theoretical and experimental π^-/π^+ ratios led Radi et al.[21] to conduct a Monte Carlo study of pion trajectories. In their model the pions are emitted only from the intersection of nuclear surfaces. Pions traveling through the spectators are absorbed and removed from the calculation. The model gives a good prediction of the π^-/π^+ ratios: theory predicts ratios of 1.68 and 1.75 for Ne + NaF and Ar + Ca, respectively, while we obtain 1.76 ± 0.1 and 1.5 ± 0.2 from the data at zero energy in the center of mass. These ratios are similar to the transparency model of Libbrecht and Koonin, in which the nuclei pass through each

other without forming a fireball. However a complete transparency model would not be consistent with observed proton spectra.[20]

Harris et al.[22] report π^-/π^+ ratios near unity and fairly flat spectra for $^{40}Ca + {}^{40}Ca$ at 1.05 A GeV.

IV. Conclusion

Data have been presented for production of low energy (CM) pions for 655 and 1050A MeV heavy ion beams. The $^{40}Ar + Ca \rightarrow \pi^+$ data are in reasonable overall agreement with those of Wolf et al.[1] although there are some disagreements with reflected data. Further experimentation would be desirable to resolve these differences. A mid-rapidity π^- peak is observed in the Ne + NaF experiment. This result shows that more than simple Coulomb effects are needed to explain the mid-rapidity pion bumps.

Further experiments are in progress that may help decide which explanations are correct.[24] In these experiments pion spectra from central and varying degrees of peripheral collisions are measured.

V. Acknowledgements

We thank M. Gyulassy and S. Koonin for helpful discussions.

This work was supported by the Director, Office of Energy Research, Division of Nuclear Physics of the Office of High Energy and Nuclear Physics, and in part by the Director, Office of Energy, Health, and Environmental Research, of the U.S. Department of Energy

under Contract DE-AC03-76SF00098, by the INS-LBL collaboration program, Institute for Nuclear Study, University of Tokyo, Japan, and by the U.S. National Science Foundation under Grant No. PHY 78-22696.

References

(1) K.L. Wolf, H.H. Gutbrod, W.G. Meyer, A.M. Poskanzer, A. Sandoval, R. Stock, J. Gosset, C.H. King, G. King, Nguyen Van Sen, G.D. Westfall, Phys. Rev. Lett. 42, 1448 (1979). Also see: K.L. Wolf, H.H. Gutbrod, W.G. Meyer, A.M. Poskanzer, A. Sandoval, R. Stock, J. Gosset, J.-C. Jourdain, C.H. King, G. King, Nguyen Van Sen, G.D. Westfall, Phys. Rev. C26, 2572 (1982).

(2) J. Chiba, K. Nakai, I. Tanihata, S. Nagamiya, H. Bowman J. Ingersoll, J.O. Rasmussen, Phys. Rev. C20, 1332 (1979).

(3) K.A. Frankel, J.A. Bistirlich, R. Bossingham, H.R. Bowman, K.M. Crowe, C.J. Martoff, D. Murphy, J.O. Rasmussen, J.P. Sullivan, W.A. Zajc, J.P. Miller, O. Hashimoto, M. Koike, J. Péter, W. Benenson, G.M. Crawley, E. Kashy, J.A. Nolen,Jr., J. Quebert, Phys. Rev. C25, 1102 (1982).

(4) D. Cochran, P. Dean, R. Gram, E. Knapp, E. Martin, D. Nagle, R. Perkins, W. Shlaer, H. Thiessen, E. Theriot, Phys. Rev. D6, 3085 (1972).

(5) K. Nakai, J. Chiba, I. Tanihata, M. Sasao, H. Bowman, S. Nagamiya, J.O. Rasmussen, Phys. Rev. C20, 2210 (1979).

(6) J. Sullivan and J.O. Rasmussen, Bull. Am. Phys. Soc., 23, 956 (1978).

(7) Y. Yariv and Z. Fraenkel, Phys. Rev. C24, 488 (1981).

(8) K.G. Libbrecht and S.E. Koonin, Phys. Rev. Lett. 43, 1581 (1979).

(9) J. Cugnon and S.E. Koonin,Nucl. Phys. A355, 477 (1981).

(10) M. Gyulassy and S.K. Kauffmann, Nucl. Phys. A362, 503 (1981).

(11) C.M. Ko and P.J. Siemens, Nucl. Phys. A367, 496 (1981).

(12) W. Benenson, G. Bertsch, G.M. Crawley, E. Kashy, J.A. Nolen, Jr., H. Bowman, J.G. Ingersoll, J.O. Rasmussen, J. Sullivan, M. Koike, M. Sasao, J. Péter, T.E. Ward, Phys. Rev. Lett. 43, 683 (1979) ; errata: 44, 54 (1980)

(13) J.P. Sullivan, J.A. Bistirlich, H.R. Bowman, R. Bossingham, T. Buttke, K.M. Crowe, K.A. Frankel, C.J. Martoff, J. Miller, D.L. Murphy, J.O. Rasmussen, W.A. Zajc, O. Hashimoto, M. Koike, J. Péter, W. Benenson, G.M. Crawley, E. Kashy, J.A. Nolen, Jr., Phys. Rev. C25, 1499 (1982)

(14) H.M.A. Radi, J.O. Rasmussen, J.P. Sullivan, K.A. Frankel, O. Hashimoto, Phys. Rev. C25, 1518 (1982).

(15) H. Kitazoe and M. Sano, Lett. Nuovo. Cim. 14, 400 (1975).

(16) J. Zimanyi, G. Fai, and B. Jakobsson, Phys. Rev. Lett. 43, 1705 (1979).

(17) J.O. Rasmussen, Nucl. Phys. A400, 383c (1983).

(18) T.E.O. Ericsson and F. Myhrer, Phys. Lett. 74B, 163 (1978).

(19) V.B. Mandelzweig, A. Gal, and E. Friedman, Ann. Phys.(N.Y.) 124, 124 (1980).

(20) S. Nagayima, M.-C. Lemaire, E. Moeller, S. Schnetzer, G. Shapiro, H. Steiner, and I. Tanihata, Phys. Rev. C24, 971(1981).

(21) Hafez M.A. Radi, John O. Rasmussen, Kenneth A. Frankel, John P. Sullivan, and H.C. Song, Phys. Rev. C27, 606 (1983).

(22) J.W. Harris, R. Brockmann, K.L. Wolf, E.K. Jackson, J. Miller, H.G. Pugh, P. Renteln, G. Roche, L.S. Schroeder, R.N. Treuhaft, G.Krebs, and P. Kirk, Nuclear Science Division Annual Report, 1983-1984, Lawrence Berkeley Laboratory, Berkeley, CA 94720; and Lawrence Berkeley Laboratory Report LBL-18635.

(23) J.A. Bistirlich, K.M. Crowe, H. Hamagaki, T.J. Humanic, T. Kobayashi, S. Nagamiya, K. Nakayama, J.O. Rasmussen, Y. Shida, I. Tanihata, O. Yamakawa, and N. Yoshikawa, Nuclear Science Division Annual Report, 1983-1984, Lawrence Berkeley Laboratory, Berkeley, CA 94720; and Lawrence Berkeley Laboratory Report LBL-18635.

Figure Captions

Fig. 1. Schematic diagram of the spectrometer in the 0° position.

Fig. 2a. Lorentz invariant cross section vs. lab momentum for Ar + C $\rightarrow \pi^-$ at 1026 A MeV. Each set of data is at a fixed laboratory angle, which is shown on the right side of the figure. A cross section offset has been added to the data at each angle, which is also given on the right side of the figure. The straight lines are drawn only to guide the eye. The velocity of the incident beam corresponds to 254 MeV/c pions.

Fig. 2b. Lorentz invariant cross section vs. lab momentum for Ar + C $\rightarrow \pi^+$ at 1026 A MeV. See also the caption for Fig. 2a.

Fig. 3a. Lorentz invariant cross section vs. lab momentum for Ar + Ca $\rightarrow \pi^-$ at 1020 A MeV See also the caption for Fig.2a.

Fig. 3b. Lorentz invariant cross section vs. lab momentum for Ar + Ca $\rightarrow \pi^+$ at 1020 A MeV. See also the caption for Fig. 2a.

Fig. 4a. Lorentz invariant cross section vs. lab momentum for Ar + U $\rightarrow \pi^-$ at 1026 A MeV. See also the caption for Fig. 2a.

Fig. 4b. Lorentz invariant cross section vs. lab momentum for Ar + U $\rightarrow \pi^+$ at 1026 A MeV. See also the caption for Fig. 2a.

Fig. 5. Lorentz invariant cross section vs. lab kinetic energy for Ar + U, Ca, and C $\rightarrow \pi^{\pm}$ at a lab angle of 15°.

Fig. 6a,b. Lorentz invariant cross section vs. lab momentum for Ne + NaF $\rightarrow \pi^-$ at 655 A MeV. Each set of data points is at a fixed lab angle, which is shown on the right side of the figure. A cross section offset has been added to the data at each angle in order to display it all on the same graph. This offset is given on the right side of the figure. The solid line is from a least squares fit of a function based on the Coulomb correction equations of Gyulassy and Kauffmann.[10] The solid line has the experimental resolution folded into it. The arrows mark the velocity of the incident beam. Details of the fitting procedure are given in ref. 14.

Fig. 6c. Lorentz invariant cross section vs. lab momentum for Ne + NaF $\rightarrow \pi^+$ at 655 A MeV. See also the caption for Figure 6ab.

Fig. 7a. Lorentz invariant cross section vs. lab momentum for Ne + Be $\rightarrow \pi^-$ at 654 A MeV. See also the caption for Figure 6ab.

Fig. 7b. Lorentz invariant cross section vs. lab momentum for Ne + Be $\rightarrow \pi^+$ at 654 A MeV. See also the caption for Fig. 6ab.

Fig. 8. The top part of the figure shows a perspective representation of the surface defined by the Lorentz invariant cross section ($Ed^3\sigma/dp^3$, units of $\mu b/sr\ MeV^2$) as a function of rapidity ($y = \tanh^{-1}(p_{\parallel}/E)$) and $p_{\perp}$ for Ne + NaF $\rightarrow \pi^-$ at 655 A MeV. The bottom part of the figure is a contour plot of the same surface with the same scales for the y and $p_{\perp}$ axes. The data were assumed to be symmetric about the center of mass rapidity, and all points have been reflected about the center of mass. Only the part of the data on the

projectile side of the center of mass has been shown.

Fig. 9. The top part of the figure shows a perspective representation of the surface defined by the Lorentz invariant cross section ($Ed^3\sigma/dp^3$, units of $\mu b/sr\ MeV^2$) as a function of rapidity ($y = \tanh^{-1}(p_{\parallel}/E)$) and $p_{\perp}$ for Ne+NaF $\rightarrow \pi^+$ at E/A = 655 MeV. The bottom part of the figure is a contour plot of the same surface with the same scales for the y and $p_{\perp}$ axes. The data were assumed to be symmetric about the center of mass rapidity and all points have been reflected about the center of mass. Only the part of the data on the projectile side of the center of mass has been shown.

Fig. 10. Lorentz invariant cross section vs. center-of-mass rapidity for 1020 A MeV Ar + Ca $\rightarrow \pi^{\pm}$ at 0°, and Lorentz invariant cross section vs. the perpendicular component of lab momentum ($p_{\perp}$) for 1020 A MeV Ar + Ca $\rightarrow \pi^{\pm}$ at the center-of-mass rapidity, y = 0.69.

Fig. 11. Pion invariant production cross sections for Ne + NaF at E/A = 655 A MeV at 0° and 90° (CM). Data for π^- are shown as open circles and π^+ as solid dots. To insure adequate statistics we took the cross section as an average not over a fixed angle (CM) but rather over a fixed interval ±0.05 in rapidity y_{CM}.

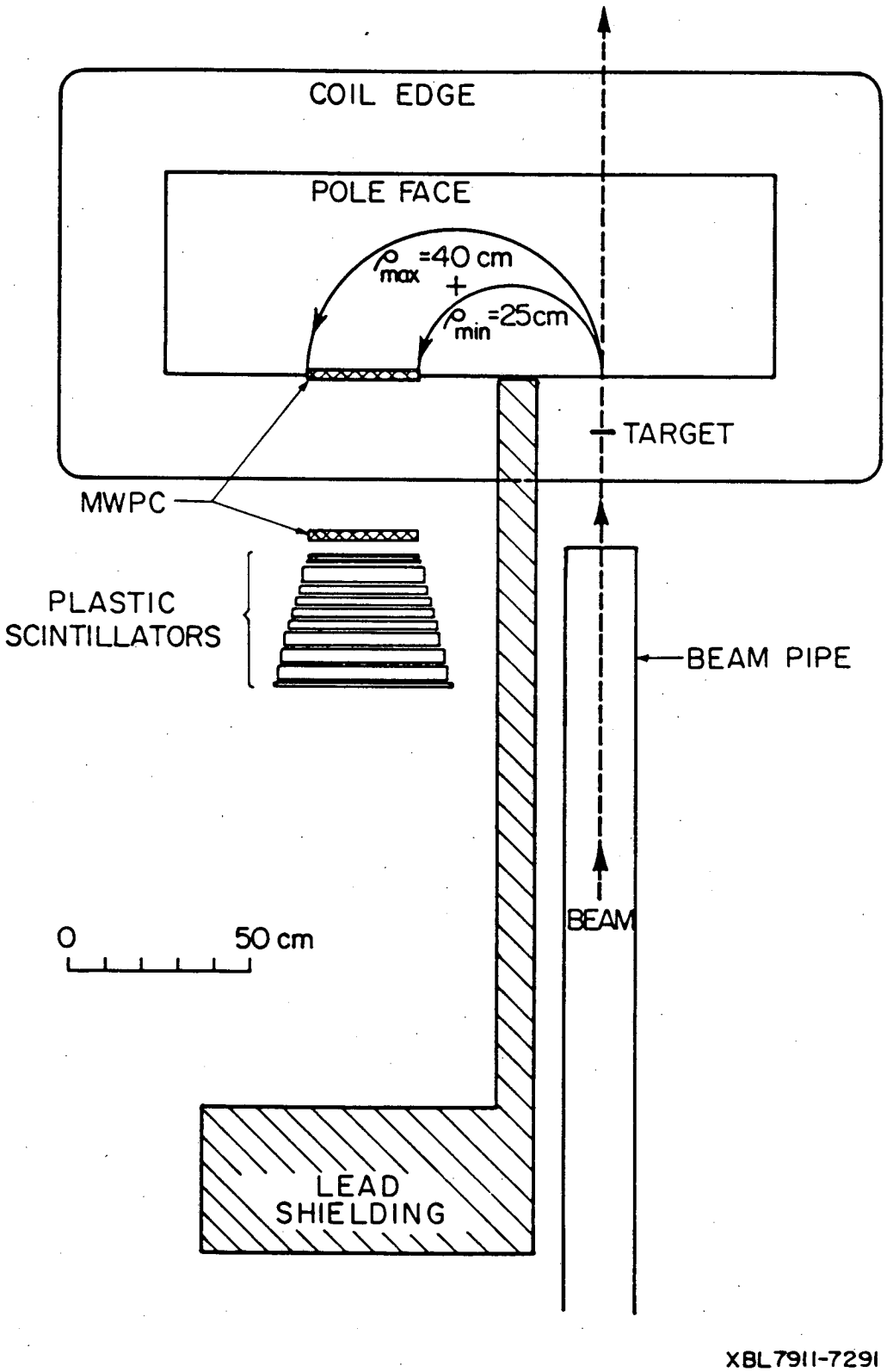
COIL EDGE
POLE FACE
ρ_{max} =40 cm
+
ρ_{min} =25cm
TARGET
MWPC
PLASTIC
SCINTILLATORS
BEAM PIPE
BEAM
0
50 cm
LEAD
SHIELDING
XBL7911-7291

Fig. 1

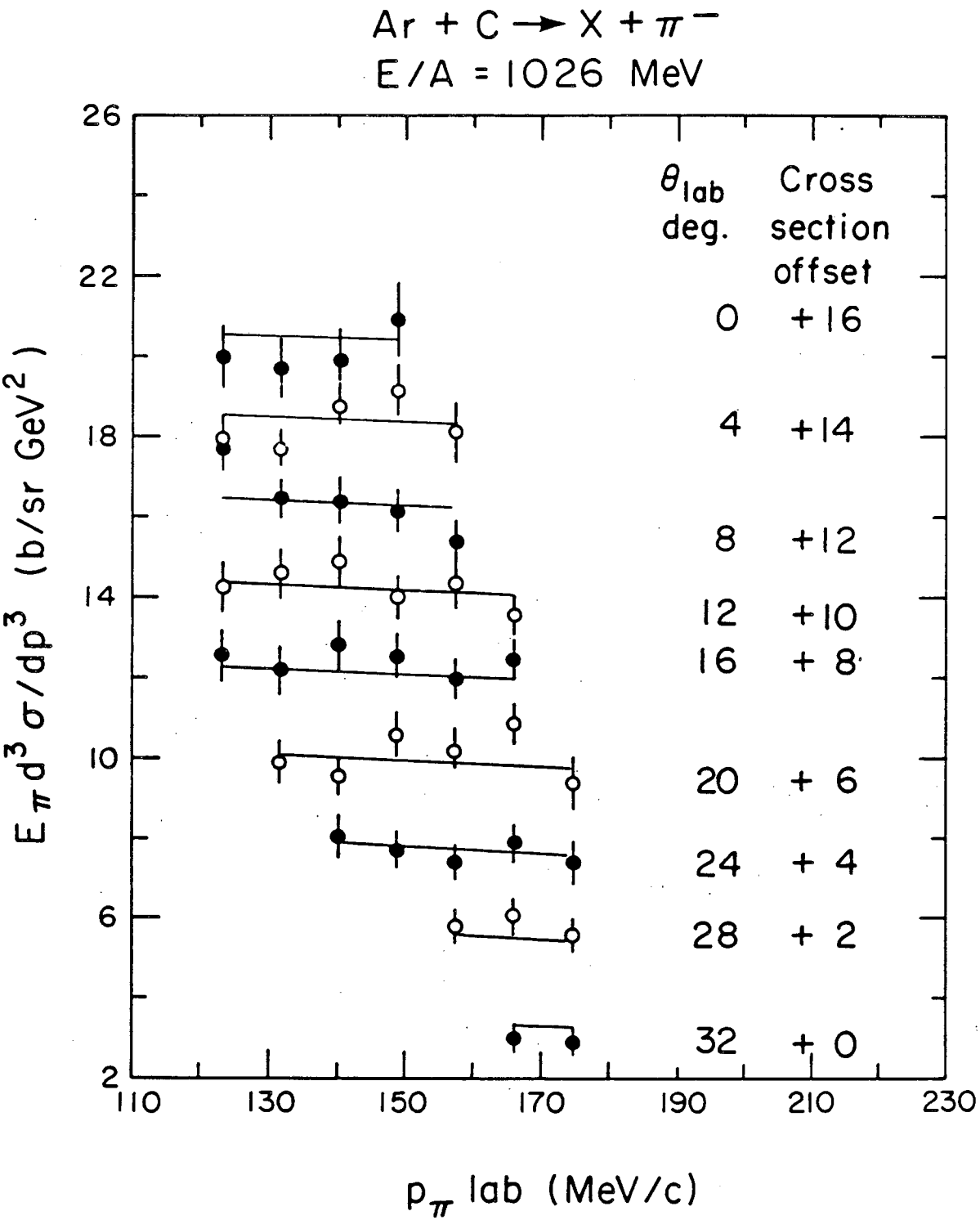

XBL 829 – 1136

Fig. 2a

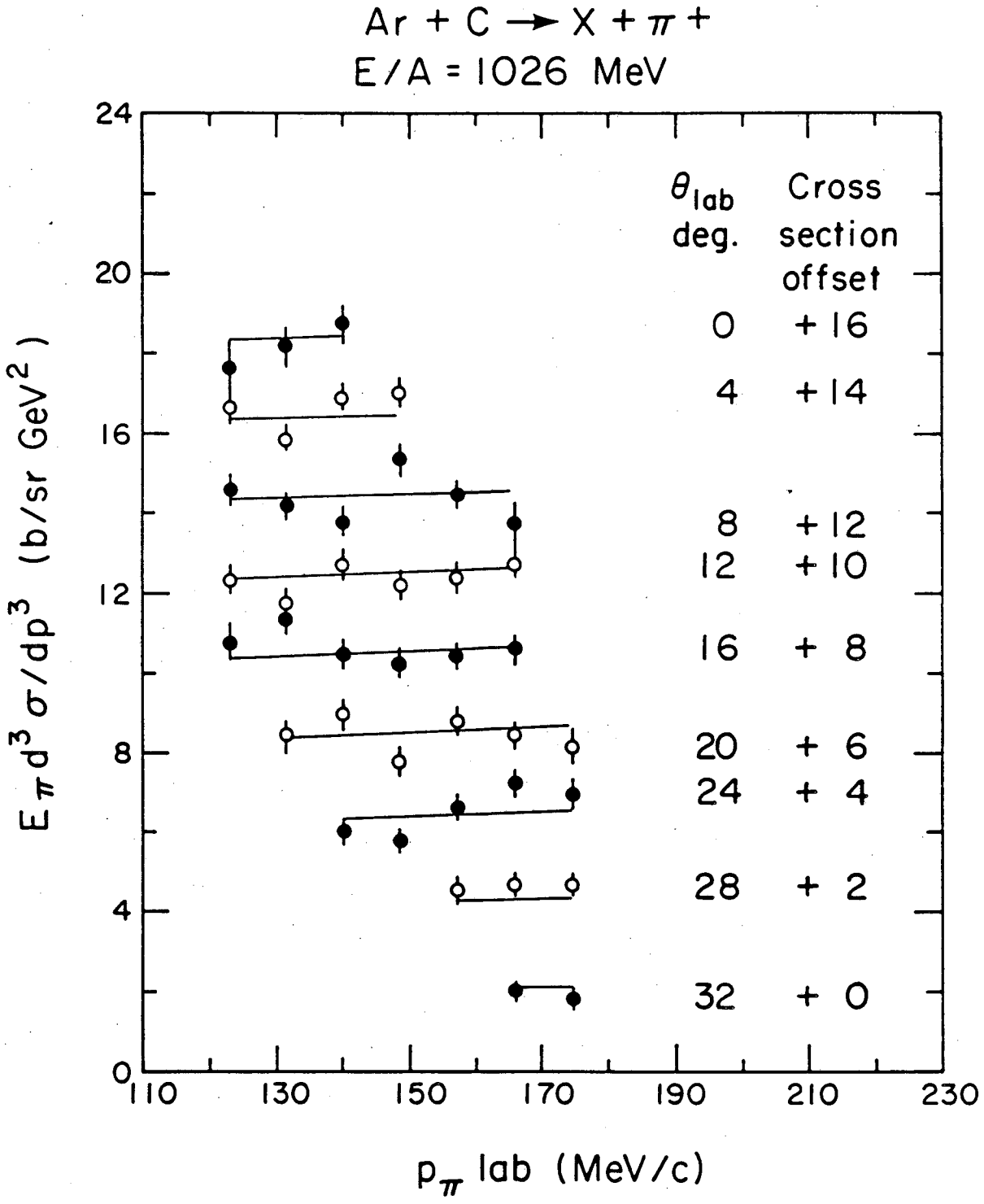

XBL 829 – 1137

Fig. 2b

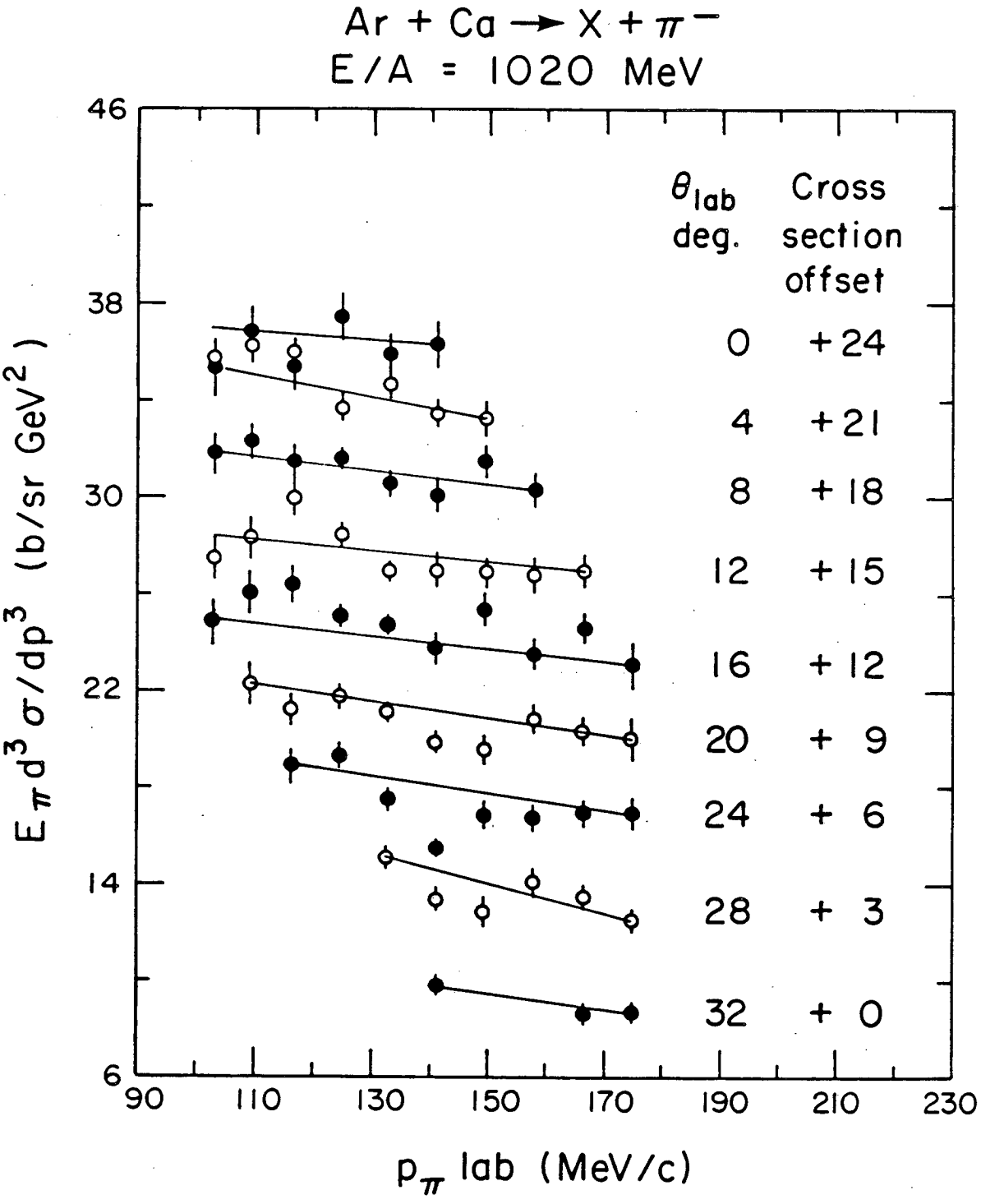

XBL 829 – 1134

Fig. 3a

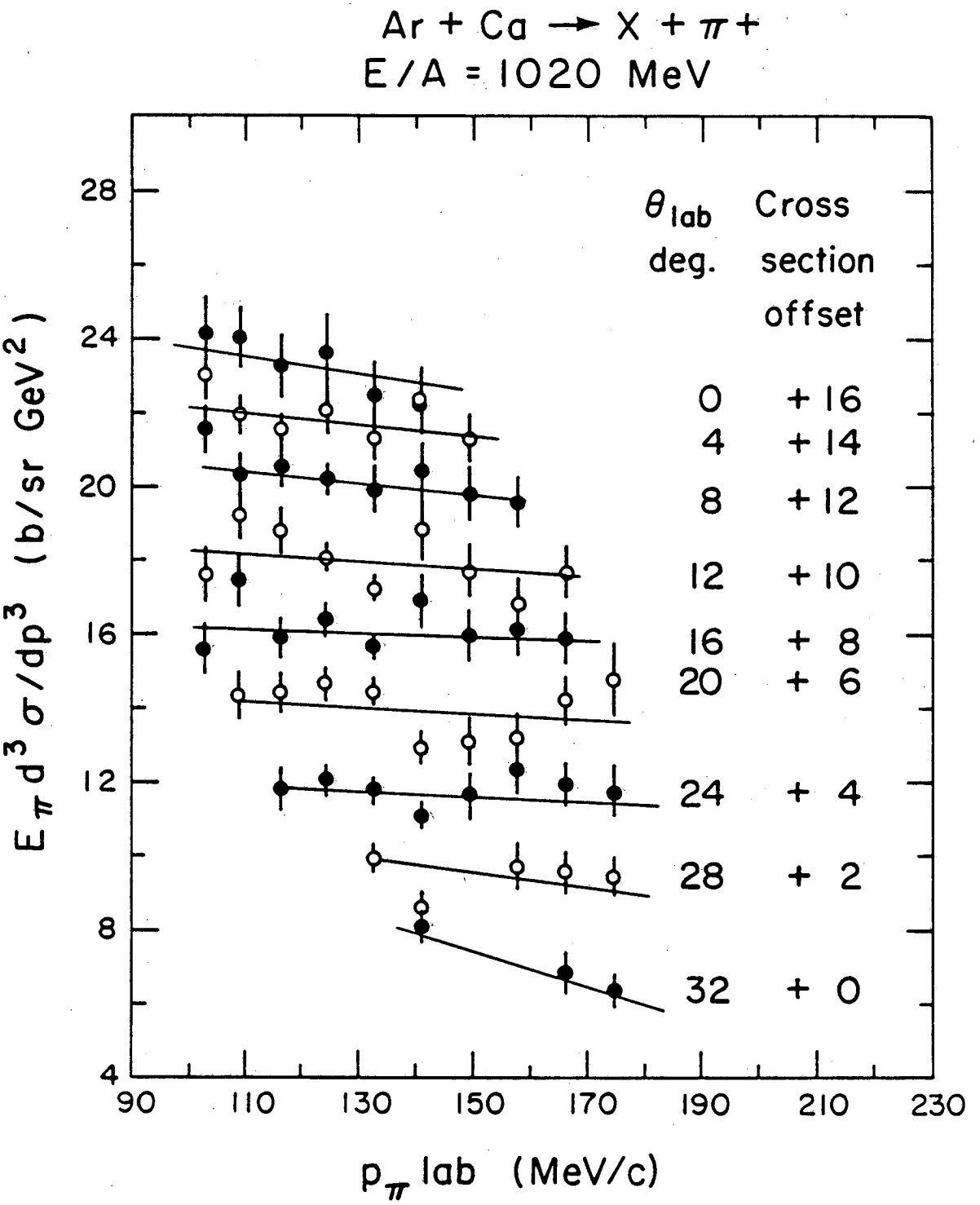

XBL 829 – 1139

Fig. 3b

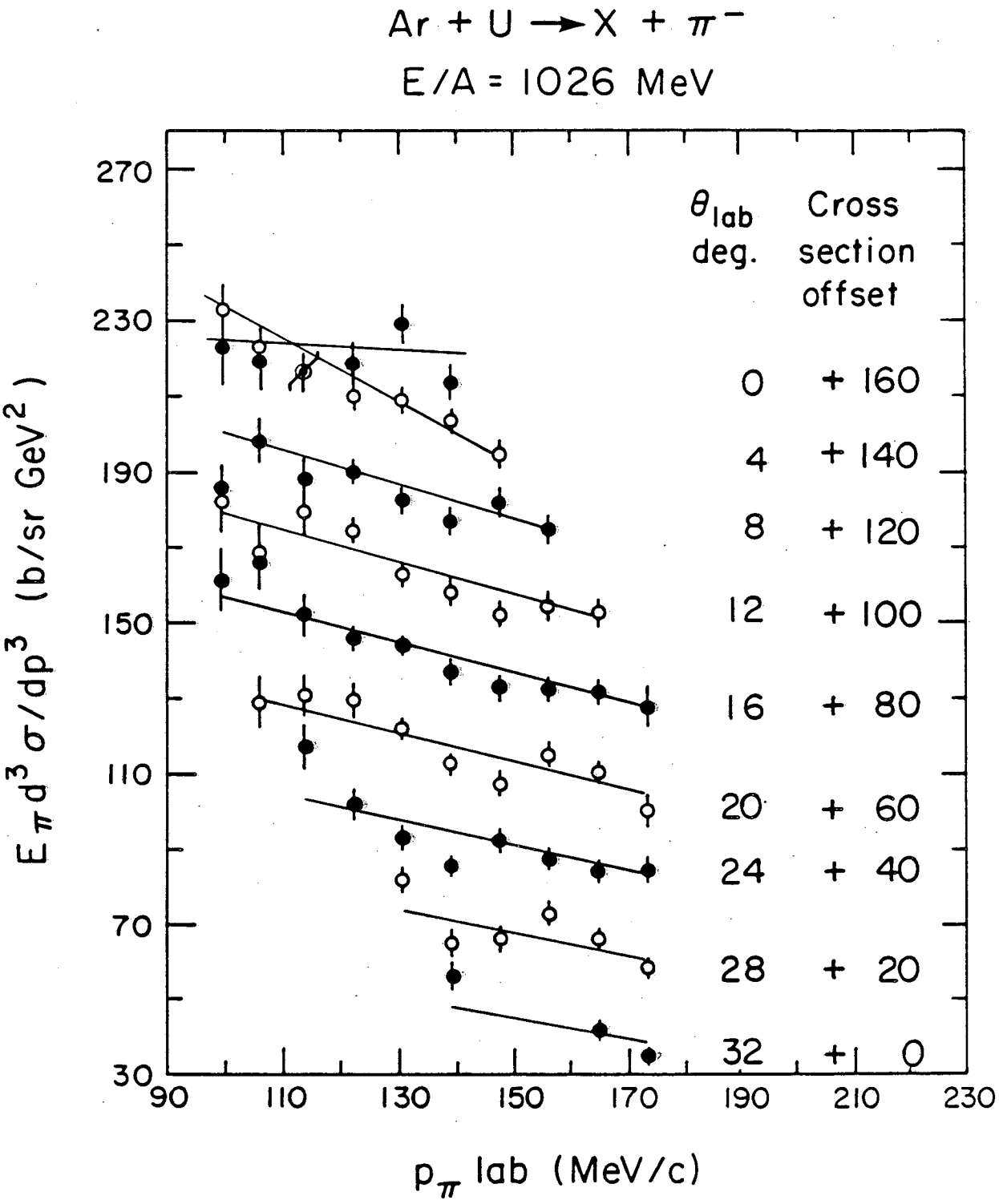
Ar + U → X + π⁻
E/A = 1026 MeV
θlab deg.
Cross section offset
0 + 160
4 + 140
8 + 120
12 + 100
16 + 80
20 + 60
24 + 40
28 + 20
32 + 0
270
230
190
150
110
70
30
90
110
130
150
170
190
210
230
Eπ d³σ/dp³ (b/sr GeV²)
pπ lab (MeV/c)
XBL 829 – 1135

Fig. 4a

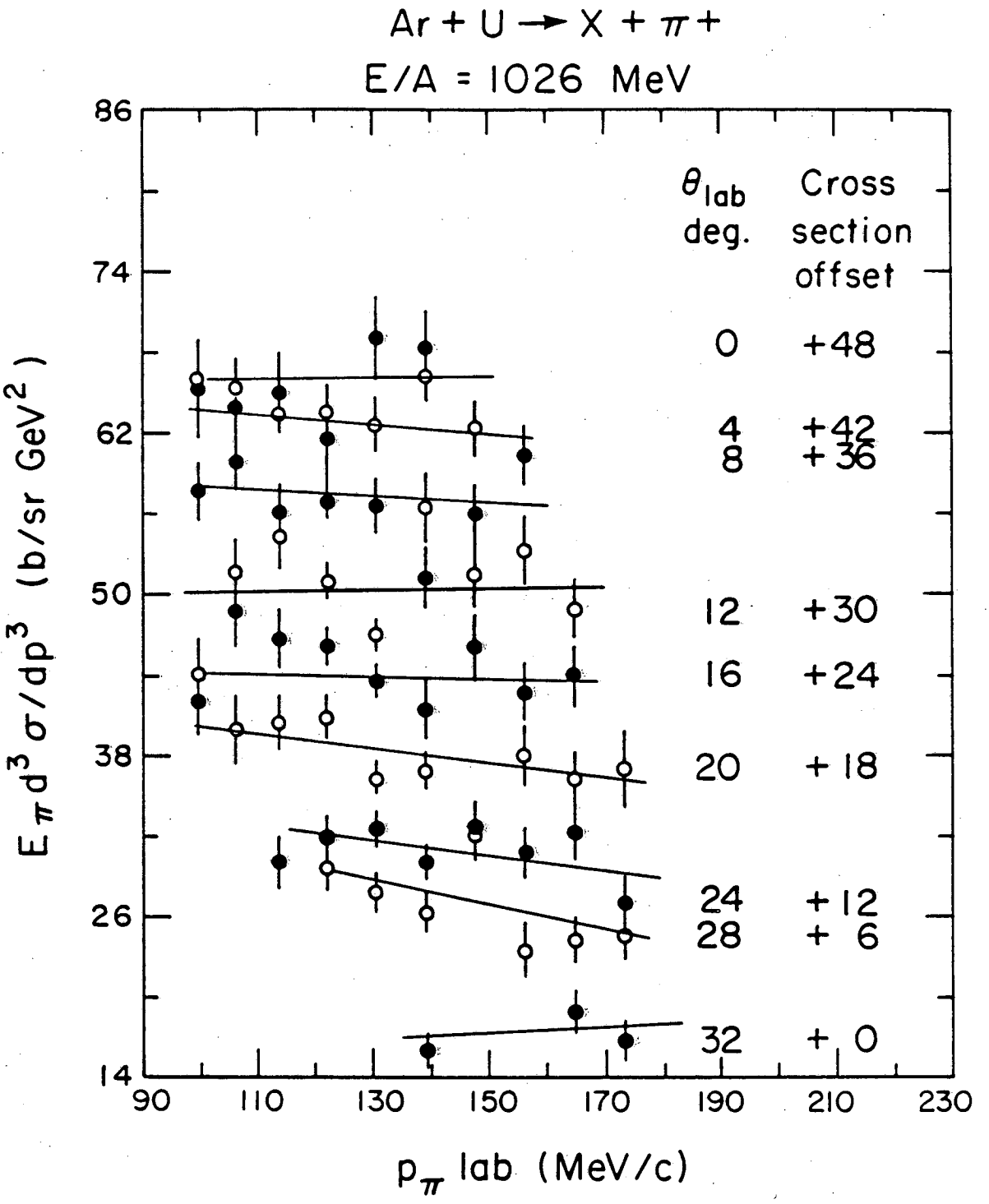

XBL 829 – 1138

Fig. 4b

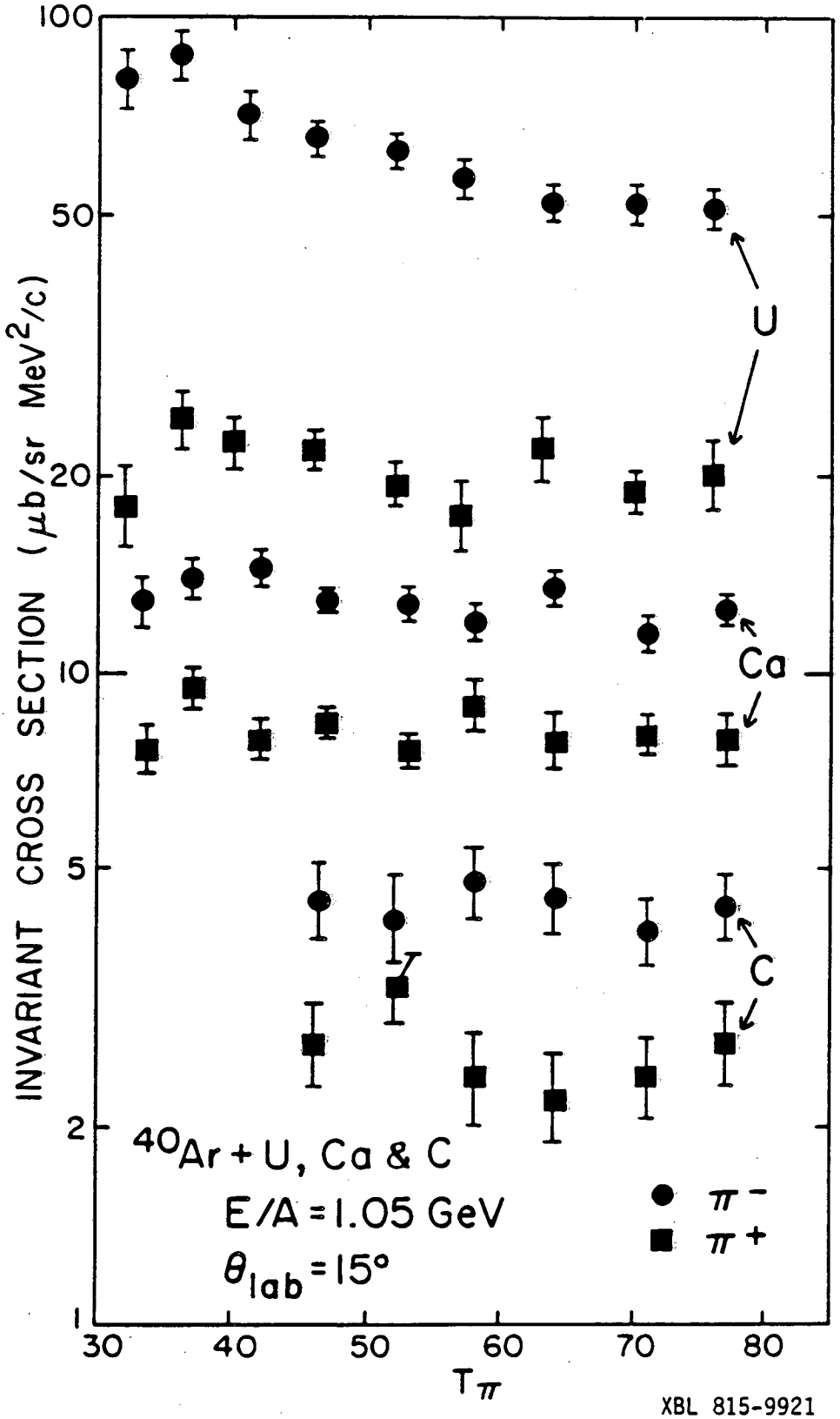
INVARIANT CROSS SECTION (μb/sr MeV²/c)
100
50
20
10
5
2
1
30
40
50
60
70
80
Tπ
U
Ca
C
40Ar + U, Ca & C
E/A = 1.05 GeV
θlab = 15°
π⁻
π⁺
XBL 815-9921

Fig. 5

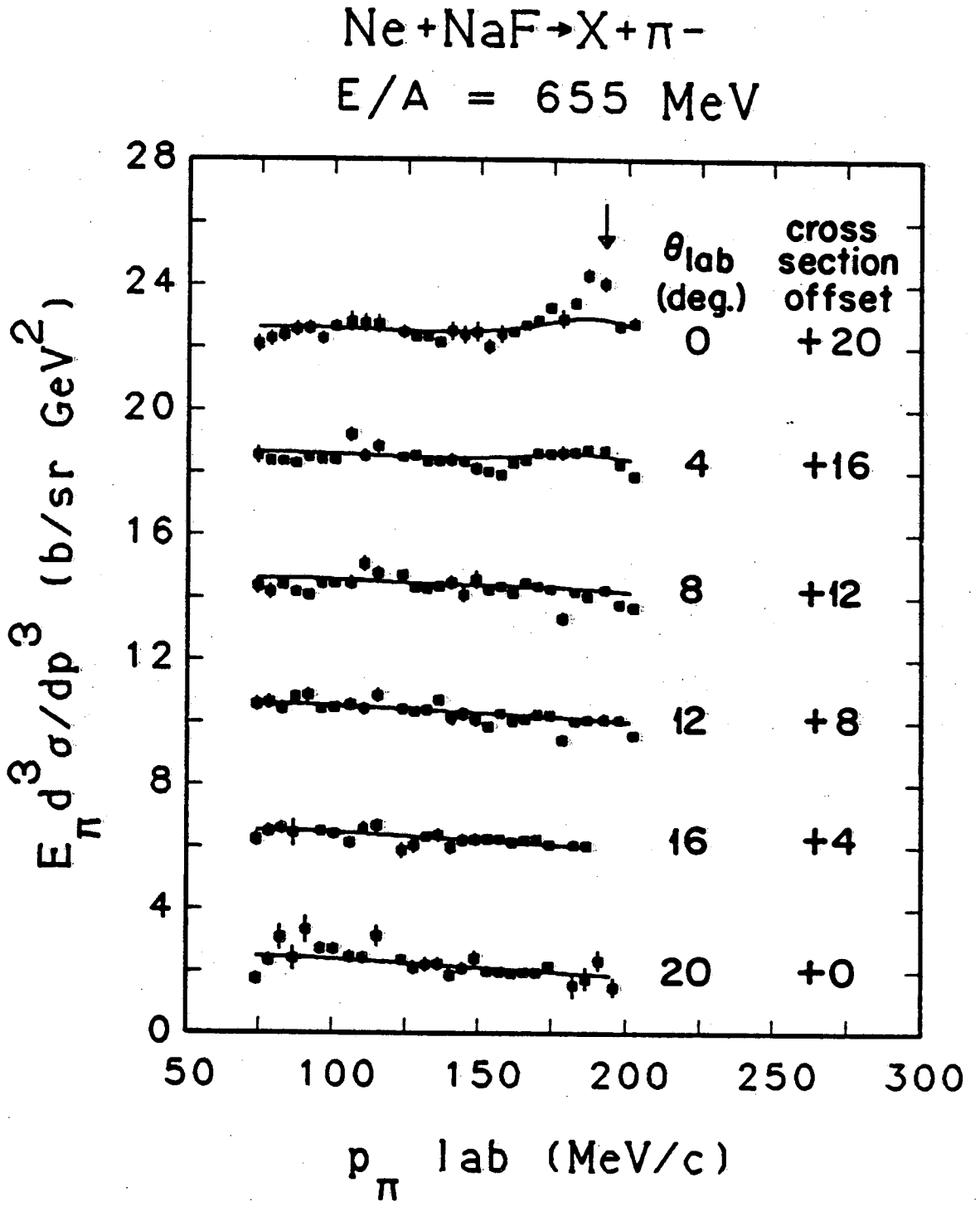
Ne+NaF→X+π-
E/A = 655 MeV
$E_\pi d^3\sigma/dp^3$ (b/sr GeV^2)
p_π lab (MeV/c)
θlab (deg.)
cross section offset
0 +20
4 +16
8 +12
12 +8
16 +4
20 +0
0
4
8
12
16
20
24
28
50
100
150
200
250
300
XBL 8112-12883

Fig. 6a

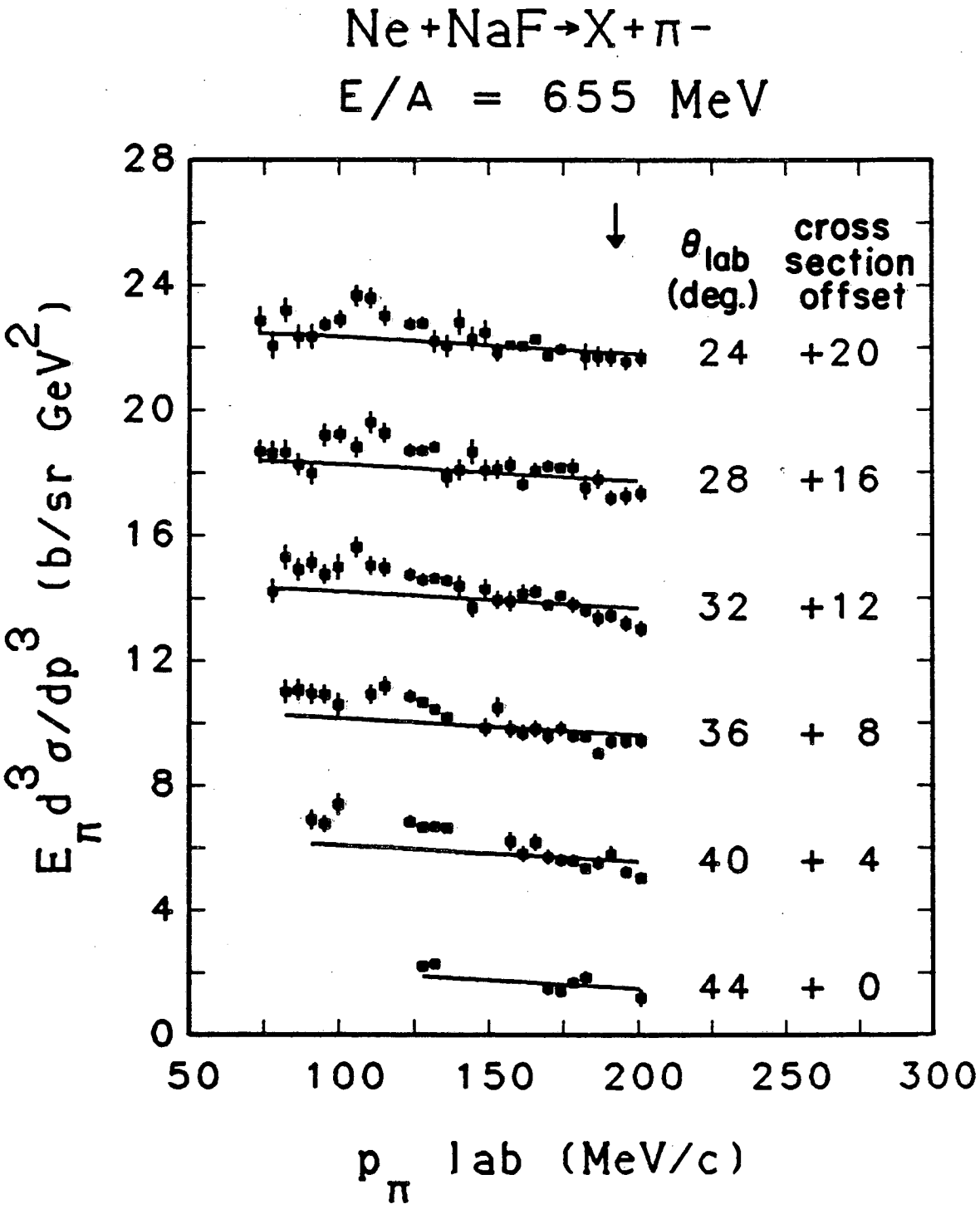
Ne+NaF→X+π-
E/A = 655 MeV
$E_\pi d^3\sigma/dp^3$ (b/sr GeV^2)
p_π lab (MeV/c)
θlab (deg.)
cross section offset
24 +20
28 +16
32 +12
36 + 8
40 + 4
44 + 0
0
4
8
12
16
20
24
28
50
100
150
200
250
300
XBL8112-12885

Fig. 6b

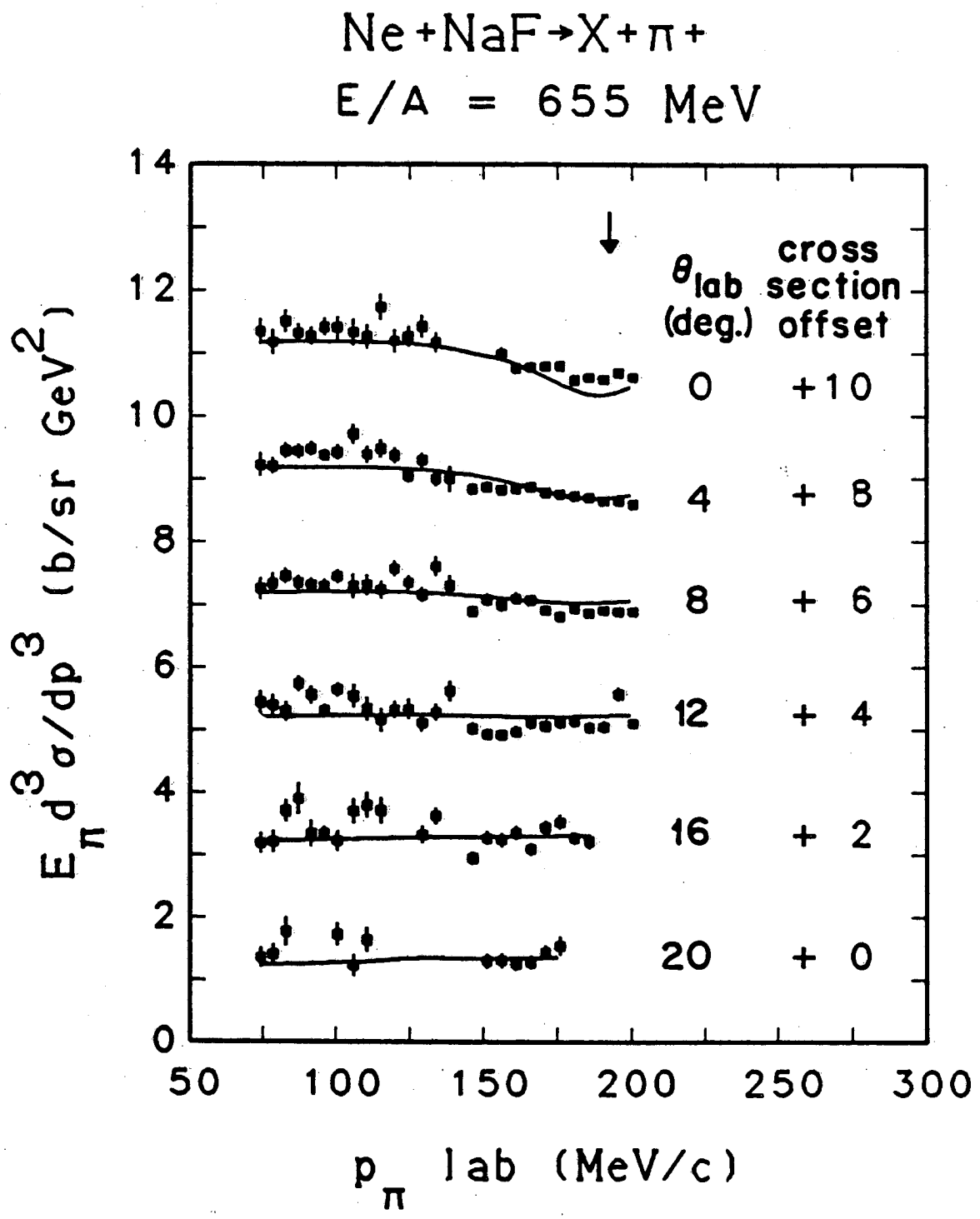
Ne+NaF→X+π+
E/A = 655 MeV
$E_\pi d^3\sigma/dp^3$ (b/sr GeV^2)
p_π lab (MeV/c)
θ_{lab} (deg.)
cross section offset
0 +10
4 + 8
8 + 6
12 + 4
16 + 2
20 + 0
0
2
4
6
8
10
12
14
50
100
150
200
250
300
XBL8112-12884

Fig. 6c

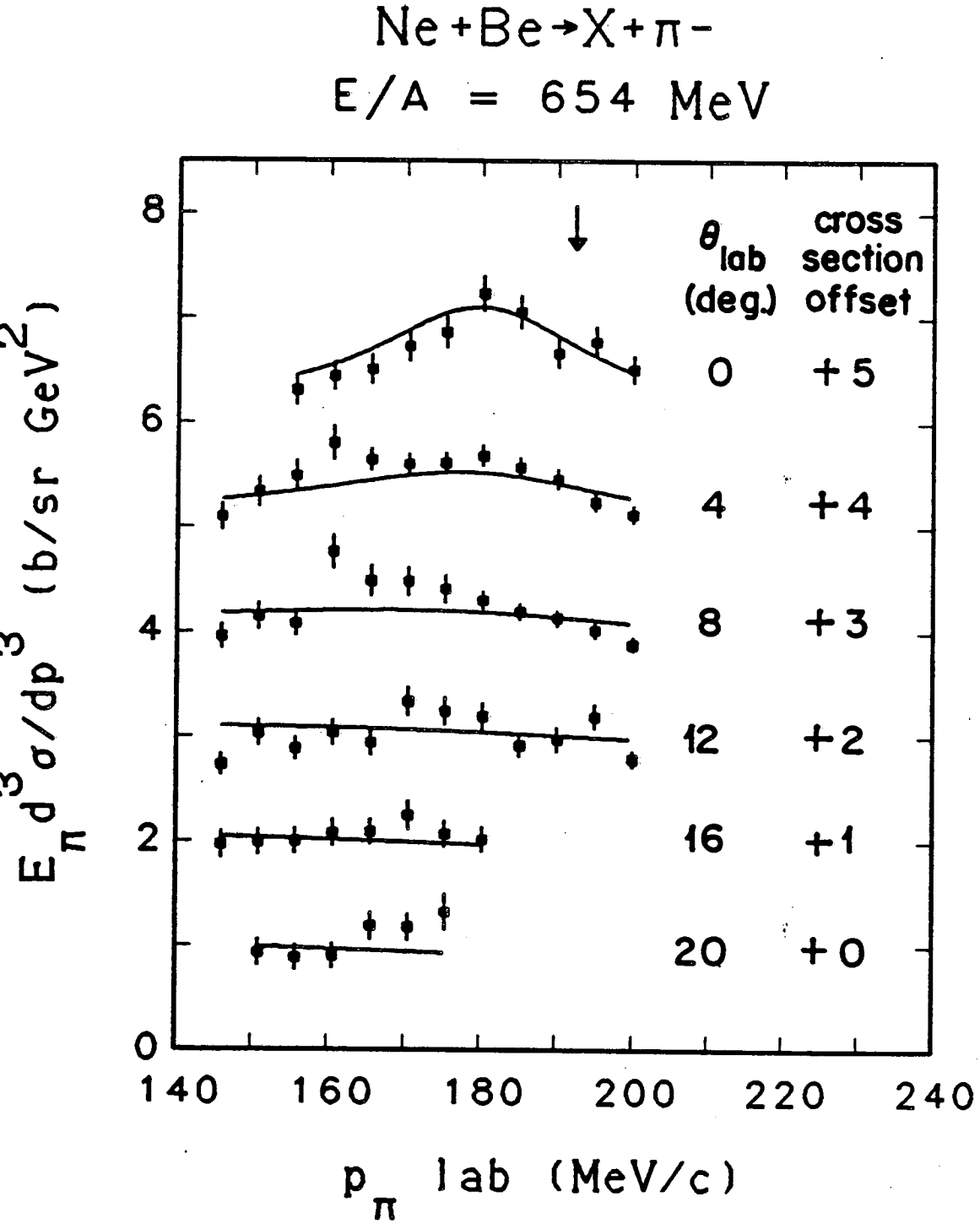
Ne+Be→X+π-
E/A = 654 MeV
θlab (deg.)
cross section offset
0 +5
4 +4
8 +3
12 +2
16 +1
20 +0
$E_\pi d^3\sigma/dp^3$ (b/sr GeV^2)
p_π lab (MeV/c)
0
2
4
6
8
140
160
180
200
220
240
XBL 8112-12682

Fig. 7a

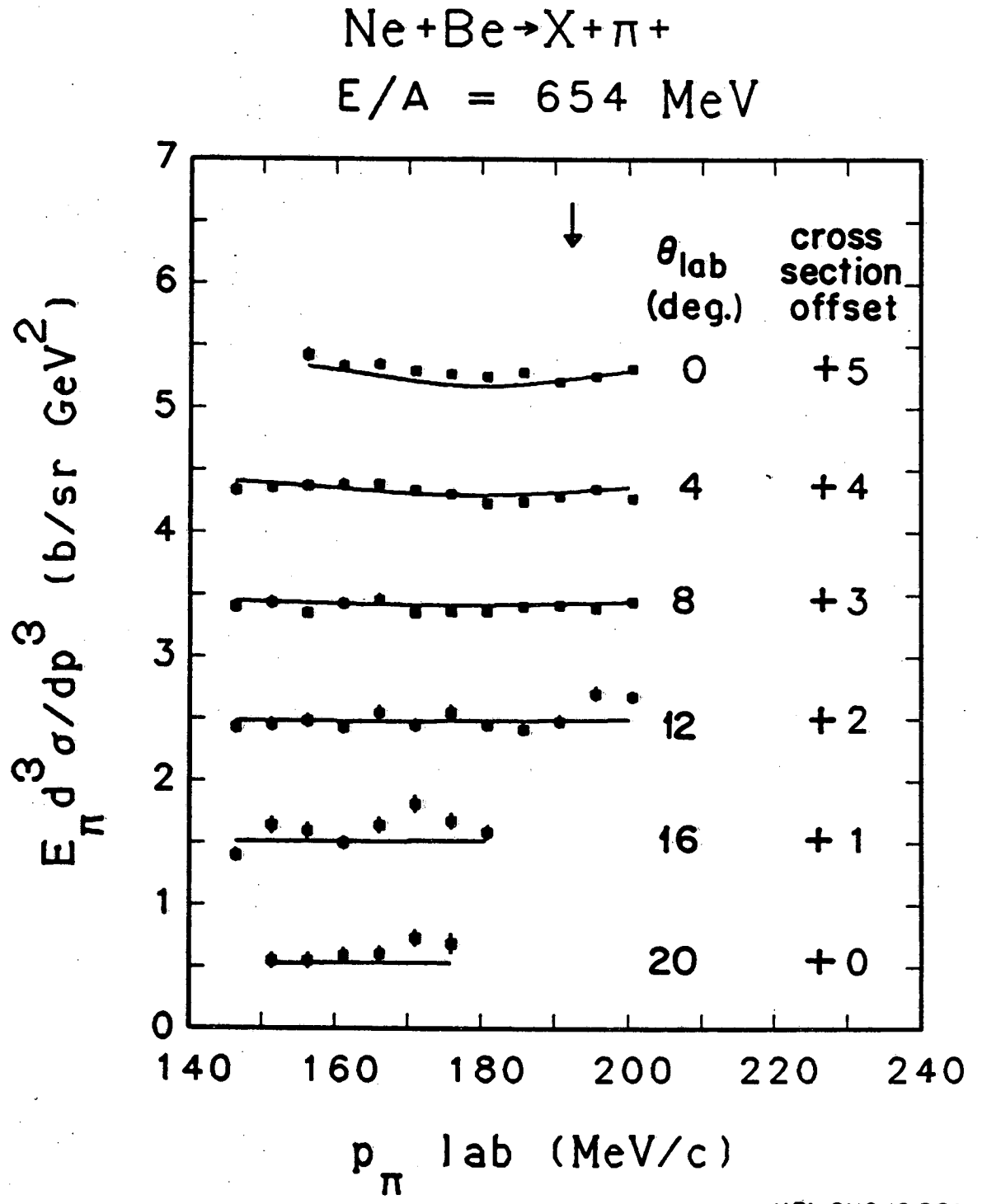
Ne+Be→X+π+
E/A = 654 MeV
θlab (deg.)
cross section offset
0
+5
4
+4
8
+3
12
+2
16
+1
20
+0
$E_\pi d^3\sigma/dp^3$ (b/sr GeV^2)
p_π lab (MeV/c)
0
1
2
3
4
5
6
7
140
160
180
200
220
240
XBL 8112-12881

Fig. 7b

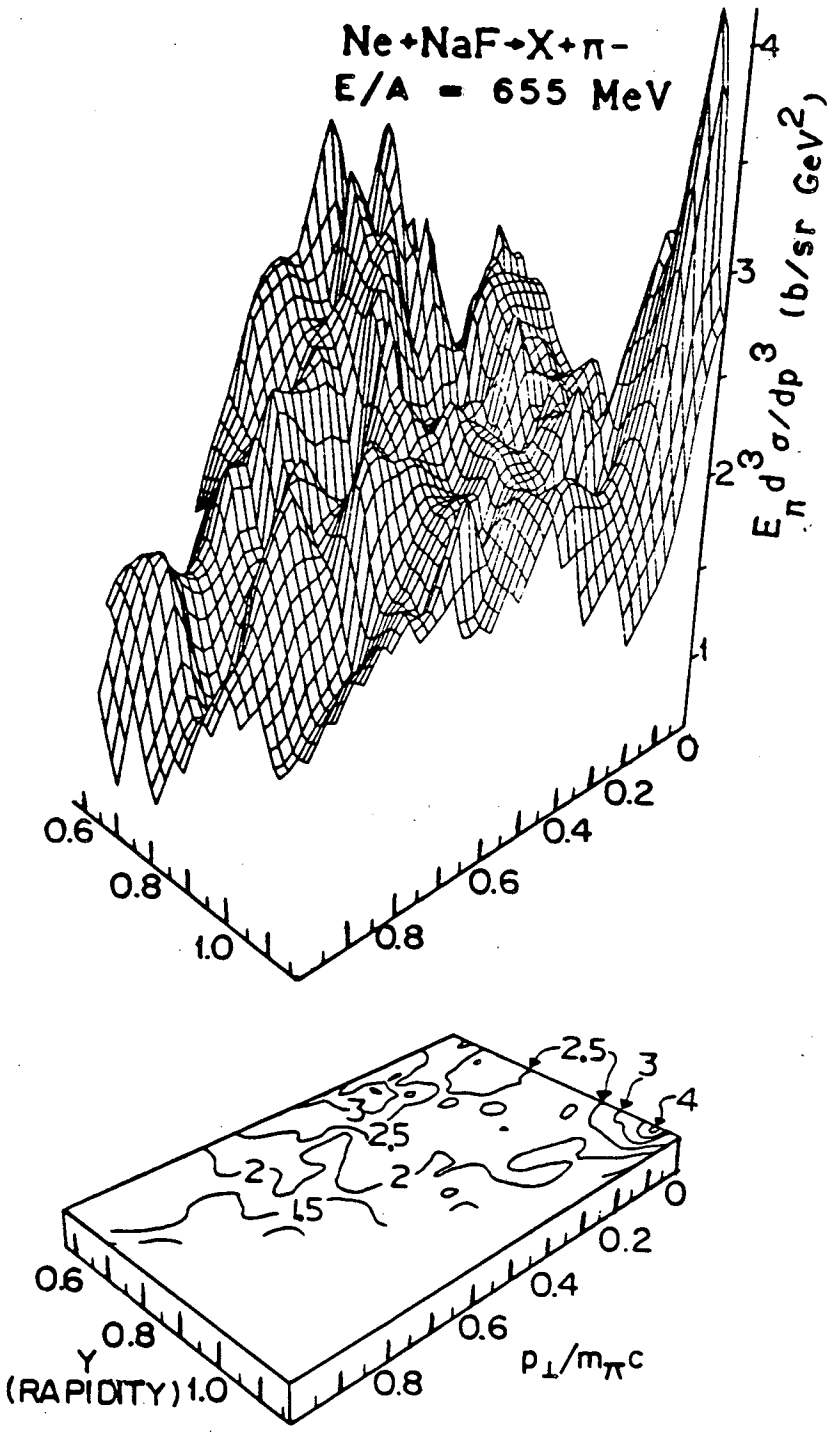

XBL8112-12886

Fig. 8

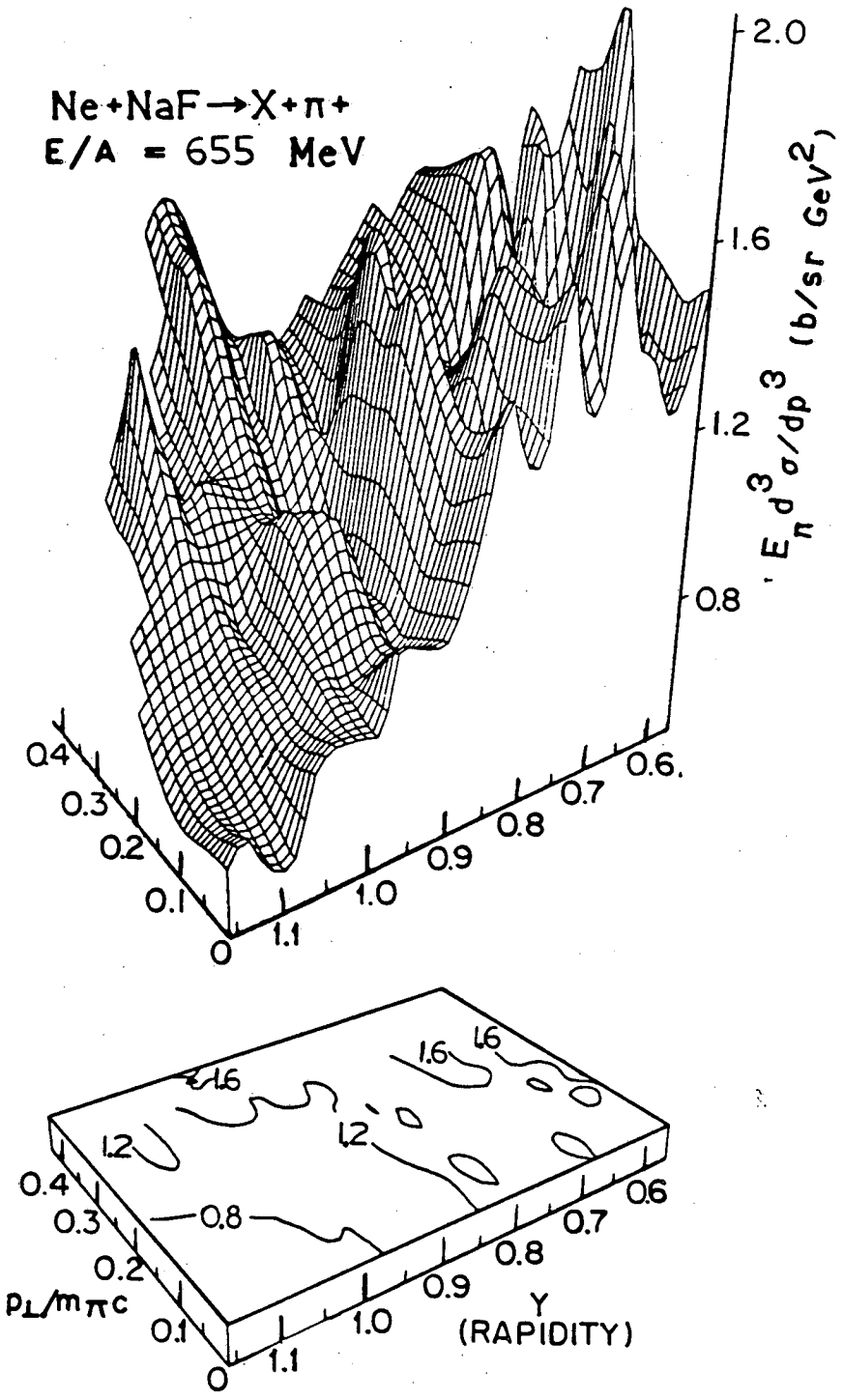

XBL8112-12887

Fig. 9

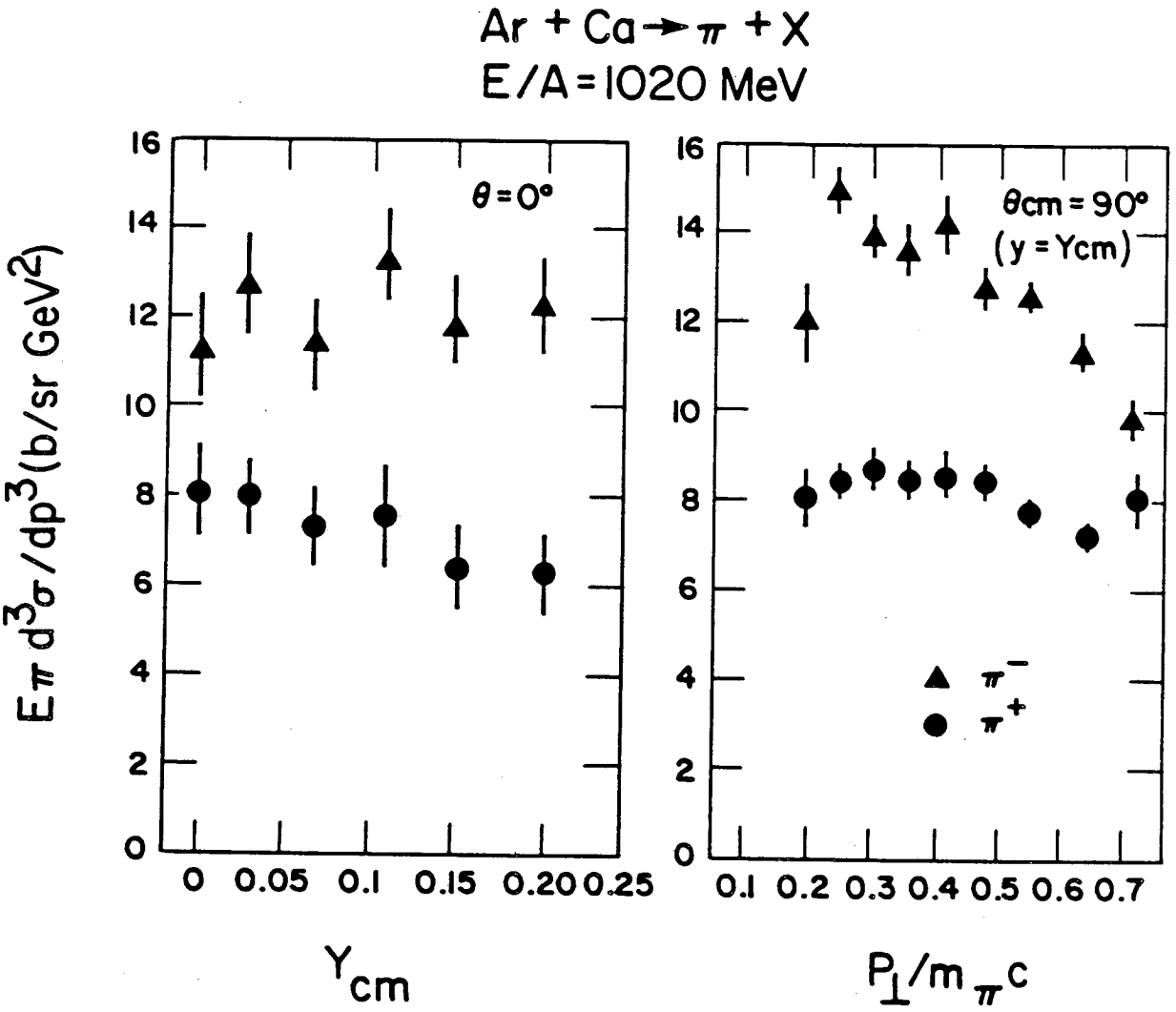

XBL 846-10651

Fig. 10

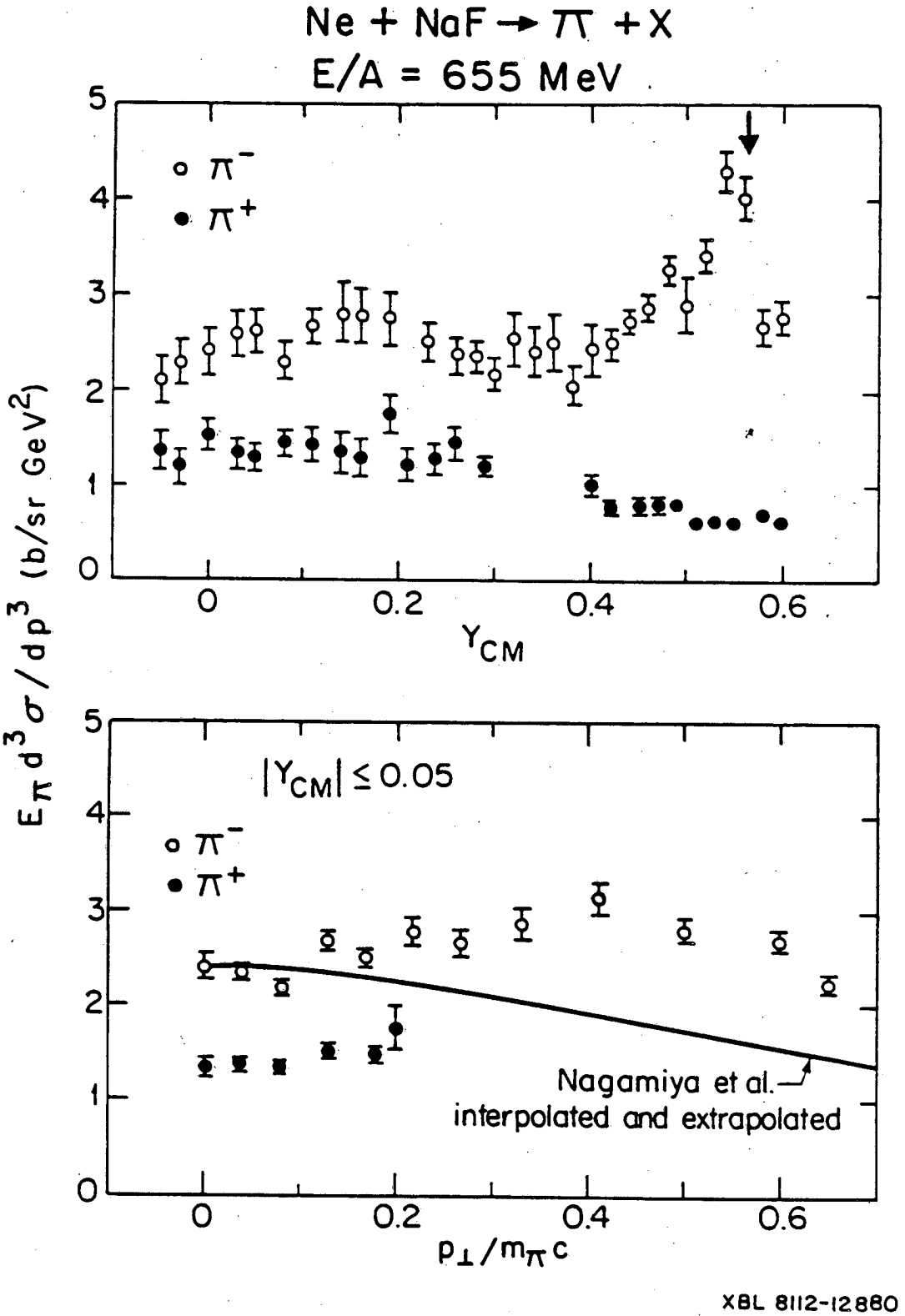
Ne + NaF → π + X
E/A = 655 MeV
π⁻
π⁺
$E_\pi d^3\sigma/dp^3$ (b/sr GeV^2)
Y_{CM}
$|Y_{CM}| \leq 0.05$
Nagamiya et al.
interpolated and extrapolated
$p_\perp/m_\pi c$
XBL 8112-12880

Fig. 11

TABLE I.

Beam Particle	Energy A Mev	Target	Thickness gm/cm^2	Central Angle Magnet (degree)	π^-/π^+** p = 0 in c.m.
^{40}Ar	1026	C	1.1	15	1.7
	1020	Ca	1.9	15	1.5
	1026	U	1.9	15	3.5
^{20}Ne	654	Be	1.1	0†	— **
	655	NaF	0.4	0,30†	1.7

*The standard deviation based on counting statistics are approximately 5% for the π^-/π^+ ratios. The true uncertainity is greater than this which we estimate it to be approximately 15%.

**Data were not taken at this angle for p = 0 in c.m.

†Data were taken at this angle for π^-.

TABLE II

Ne+Be → π^- + X

E/A = 654 MeV

$Ed^3\sigma/dp^3$ μb $c^3/(sr\ MeV^2)$

p_π	θ_π lab. degrees					
MeV/c	0	4	8	12	16	20
146	—	1.10 ±.13	.95 ±.12	.73 ±.10	.97 ±.13	—
151	—	1.33 ±.14	1.15 ±.13	1.03 ±.12	.99 ±.13	.93 ±.13
156	1.31 ±.15	1.49 ±.15	1.08 ±.12	.88 ±.11	1.00 ±.12	.89 ±.12
161	1.44 ±.14	1.80 ±.17	1.76 ±.16	1.03 ±.12	1.08 ±.13	.90 ±.12
166	1.50 ±.14	1.64 ±.11	1.49 ±.15	.94 ±.12	1.09 ±.13	1.19 ±.13
170	1.73 ±.15	1.60 ±.10	1.48 ±.14	1.34 ±.14	1.25 ±.14	1.18 ±.13
175	1.86 ±.15	1.61 ±.10	1.41 ±.14	1.24 ±.14	1.07 ±.13	1.32 ±.18
180	2.23 ±.17	1.68 ±.10	1.30 ±.09	1.19 ±.13	1.02 ±.12	—
185	2.05 ±.16	1.57 ±.10	1.19 ±.08	.92 ±.11	—	—
190	1.66 ±.15	1.46 ±.09	1.14 ±.08	.97 ±.12	—	—
195	1.77 ±.14	1.24 ±.08	1.02 ±.07	1.19 ±.11	—	—
200	1.51 ±.13	1.12 ±.08	.88 ±.07	.79 ±.08	—	—

TABLE IIIa

Ne+NaF → π^- + X

E/A = 655 MeV

$Ed^3\sigma/dp^3$

$\mu b\ c^3/(sr\ MeV^2)$

p_π	θ_π lab. degrees					
MeV/c	0	4	8	12	16	20
74	2.10 ±.25	2.55 ±.26	2.36 ±.25	2.56 ±.21	2.23 ±.20	1.75 ±.19
78	2.28 ±.24	2.37 ±.17	2.17 ±.23	2.62 ±.21	2.50 ±.22	2.36 ±.20
82	2.38 ±.24	2.36 ±.16	2.40 ±.16	2.43 ±.20	2.60 ±.20	3.08 ±.40
87	2.57 ±.23	2.30 ±.15	2.17 ±.14	2.80 ±.18	2.44 ±.41	2.43 ±.38
91	2.61 ±.22	2.50 ±.15	2.06 ±.14	2.86 ±.20	—	3.33 ±.43
96	2.29 ±.20	2.42 ±.13	2.45 ±.14	2.42 ±.13	2.50 ±.12	2.72 ±.20
100	2.66 ±.18	2.41 ±.17	2.45 ±.13	2.47 ±.13	2.42 ±.17	2.72 ±.18
106	2.81 ±.30	3.20 ±.21	2.45 ±.20	2.54 ±.19	2.13 ±.18	2.46 ±.19
110	2.77 ±.28	2.52 ±.19	3.06 ±.23	2.41 ±.19	2.58 ±.20	2.44 ±.19
115	2.74 ±.28	2.83 ±.19	2.77 ±.19	2.84 ±.22	2.68 ±.20	3.13 ±.32
123	2.49 ±.20	2.50 ±.12	2.72 ±.13	2.41 ±.13	1.88 ±.24	2.37 ±.16
128	2.35 ±.18	2.55 ±.11	2.30 ±.11	2.33 ±.12	2.05 ±.23	2.13 ±.21
132	2.35 ±.15	2.34 ±.11	2.27 ±.11	2.39 ±.11	2.33 ±.10	2.23 ±.21
136	2.16 ±.17	2.38 ±.14	2.36 ±.12	2.69 ±.12	2.37 ±.21	2.25 ±.21
140	2.52 ±.28	2.40 ±.20	2.46 ±.21	2.13 ±.20	1.99 ±.21	1.89 ±.20

TABLE IIIb

Ne+NaF → π^+ + X

E/A = 655 MeV

$Ed^3\sigma/dp^3$

$\mu b\ c^3/(sr\ MeV^2)$

p_π	θ_π lab. degrees					
MeV/c	0	4	8	12	16	20
144	2.40 ±.26	2.35 ±.17	2.08 ±.22	2.25 ±.20	2.21 ±.20	2.10 ±.19
149	2.49 ±.30	2.13 ±.19	2.56 ±.27	2.07 ±.21	2.23 ±.20	2.41 ±.23
153	2.03 ±.22	2.03 ±.13	2.25 ±.13	1.86 ±.13	2.25 ±.14	2.00 ±.16
157	2.42 ±.26	1.93 ±.12	2.34 ±.12	2.26 ±.13	2.24 ±.15	2.00 ±.14
161	2.51 ±.14	2.30 ±.13	2.14 ±.11	2.02 ±.10	2.15 ±.14	1.95 ±.13
165	2.71 ±.13	2.39 ±.11	2.45 ±.11	2.09 ±.10	2.21 ±.12	1.98 ±.10
170	2.87 ±.14	2.62 ±.10	2.35 ±.10	2.22 ±.10	2.23 ±.12	1.97 ±.10
174	3.27 ±.15	2.59 ±.09	2.25 ±.11	2.21 ±.10	2.06 ±.10	2.17 ±.11
178	2.90 ±.28	2.63 ±.22	1.32 ±.20	1.41 ±.16	—	—
182	3.41 ±.17	2.64 ±.12	2.17 ±.09	2.02 ±.12	2.05 ±.16	1.56 ±.40
187	4.30 ±.22	2.73 ±.11	2.02 ±.08	2.06 ±.14	2.03 ±.15	1.76 ±.36
191	4.04 ±.23	2.71 ±.13	2.23 ±.11	2.08 ±.18	—	2.35 ±.33
196	2.67 ±.18	2.25 ±.11	1.77 ±.10	2.06 ±.16	—	1.50 ±.29
201	2.76 ±.18	1.88 ±.10	1.67 ±.09	1.58 ±.11	—	—

TABLE IIIc

Ne+NaF → π^+ + X

E/A = 655 MeV

$Ed^3\sigma/dp^3$

$\mu b\ c^3/(sr\ MeV^2)$

p_π	θ_π lab. degrees					
MeV/c	24	28	32	36	40	44
74	2.84 ±.44	2.67 ±.27	—	—	—	—
78	2.05 ±.43	2.62 ±.36	2.21 ±.36	—	—	—
82	3.18 ±.38	2.65 ±.35	3.30 ±.34	3.00 ±.35	—	—
87	2.34 ±.38	2.26 ±.35	2.91 ±.34	3.05 ±.33	—	—
91	2.35 ±.38	1.98 ±.35	3.14 ±.32	2.93 ±.31	2.90 ±.30	—
96	2.73 ±.22	3.20 ±.34	2.75 ±.30	2.91 ±.29	2.77 ±.26	
100	2.89 ±.26	3.22 ±.27	2.99 ±.40	2.59 ±.35	3.38 ±.32	—
106	3.65 ±.33	2.81 ±.32	3.62 ±.32	—	—	—
110	3.56 ±.32	3.61 ±.34	3.30 ±.29	2.91 ±.29	—	—
115	3.00 ±.31	3.26 ±.30	2.96 ±.29	3.18 ±.29	—	—
123	2.74 ±.19	2.69 ±.20	2.74 ±.21	2.84 ±.19	2.83 ±.19	—
128	2.76 ±.19	2.69 ±.18	2.57 ±.19	2.64 ±.17	2.66 ±.16	2.22 ±.14
132	2.19 ±.35	2.80 ±.17	2.62 ±.17	2.43 ±.15	2.68 ±.15	2.29 ±.12
136	2.04 ±.34	1.85 ±.31	2.54 ±.18	2.18 ±.16	2.63 ±.15	—
140	2.79 ±.39	2.08 ±.33	2.38 ±.32	—	—	—

TABLE IIId

Ne+NaF → π^+ + X

E/A = 655 MeV

$Ed^3\sigma/dp^3$

$\mu b\ c^3/(sr\ MeV^2)$

p_π	θ_π lab. degrees					
MeV/c	24	28	32	36	40	44
144	2.25 ±.36	2.67 ±.39	1.69 ±.28	—	—	—
149	2.47 ±.38	2.07 ±.34	2.28 ±.32	1.84 ±.28	—	—
153	1.84 ±.28	2.10 ±.29	1.94 ±.27	2.49 ±.30	—	—
157	2.07 ±.14	2.24 ±.26	1.89 ±.31	1.79 ±.27	2.21 ±.29	—
161	2.03 ±.12	1.63 ±.21	2.13 ±.28	1.68 ±.24	1.82 ±.23	—
165	2.25 ±.13	2.07 ±.22	2.20 ±.21	1.81 ±.26	2.16 ±.25	—
170	1.71 ±.17	2.19 ±.19	1.78 ±.16	1.59 ±.24	1.71 ±.23	1.50 ±.20
174	1.94 ±.18	2.15 ±.18	2.07 ±.16	1.82 ±.22	1.62 ±.19	1.42 ±.18
178	—	2.16 ±.26	1.79 ±.23	1.58 ±.20	1.59 ±.19	1.68 ±.17
182	1.71 ±.41	1.53 ±.37	1.59 ±.18	1.57 ±.17	1.34 ±.17	1.85 ±.18
187	1.70 ±.32	1.78 ±.30	1.36 ±.26	1.02 ±.16	1.52 ±.22	—
191	1.68 ±.29	1.19 ±.22	1.45 ±.24	1.40 ±.22	1.80 ±.24	—
196	1.53 ±.25	1.25 ±.27	1.18 ±.22	1.41 ±.21	1.23 ±.18	—
201	1.66 ±.28	1.33 ±.25	1.00 ±.24	1.43 ±.23	1.04 ±.17	1.20 ±.26

TABLE IV

Ne+Be → π^+ + X

E/A = 654 MeV

$Ed^3\sigma/dp^3$ $\mu b\ c^3/(sr\ MeV^2)$

p_π MeV/c	θ_π lab. degrees 24	28	32	36	40	44
146	—	.33 ±.04	.40 ±.05	.43 ±.05	.40 ±.05	—
151	—	.36 ±.05	.43 ±.05	.45 ±.05	.64 ±.06	.55 ±.06
156	.42 ±.05	.37 ±.04	.35 ±.04	.48 ±.05	.59 ±.06	.55 ±.06
161	.33 ±.04	.38 ±.05	.43 ±.05	.43 ±.05	.50 ±.05	.59 ±.06
166	.35 ±.04	.39 ±.03	.45 ±.05	.54 ±.06	.64 ±.06	.61 ±.06
171	.29 ±.04	.33 ±.03	.35 ±.04	.44 ±.05	.81 ±.07	.73 ±.06
176	.27 ±.04	.31 ±.03	.36 ±.04	.55 ±.05	.67 ±.06	.69 ±.08
181	.25 ±.04	.23 ±.02	.36 ±.03	.45 ±.05	.58 ±.06	—
186	.28 ±.04	.24 ±.02	.40 ±.03	.41 ±.05	—	—
191	.21 ±.03	.29 ±.03	.41 ±.03	.47 ±.05	—	—
196	.25 ±.03	.35 ±.03	.39 ±.03	.70 ±.05	—	—
201	.31 ±.04	.27 ±.02	.44 ±.03	.68 ±.05	—	—

TABLE Va

Ne+NaF → π^+ + X

E/A = 655 MeV

$Ed^3\sigma/dp^3$

$\mu b\ c^3/(sr\ MeV^2)$

p_π MeV/c	θ_π lab. degrees 24	28	32	36	40	44
74	1.34 ±.20	1.23 ±.18	1.25 ±.17	1.44 ±.17	1.19 ±.16	1.36 ±.16
78	1.18 ±.19	1.21 ±.12	1.33 ±.16	1.39 ±.17	1.21 ±.16	1.41 ±.16
83	1.50 ±.17	1.45 ±.12	1.46 ±.12	1.29 ±.15	1.70 ±.17	1.41 ±.23
87	1.32 ±.15	1.45 ±.11	1.34 ±.10	1.74 ±.12	1.90 ±.25	—
92	1.28 ±.14	1.49 ±.10	1.32 ±.10	1.56 ±.13	1.34 ±.21	—
96	1.42 ±.13	1.38 ±.09	1.29 ±.10	1.31 ±.10	1.34 ±.11	—
100	1.41 ±.17	1.43 ±.12	1.45 ±.10	1.64 ±.11	1.22 ±.16	1.73 ±.17
106	1.33 ±.21	1.72 ±.15	1.29 ±.19	1.54 ±.18	1.70 ±.19	1.24 ±.17
110	1.27 ±.19	1.39 ±.13	1.31 ±.16	1.34 ±.18	1.79 ±.20	1.64 .19
115	1.73 ±.20	1.49 ±.14	1.24 ±.13	1.15 ±.18	1.71 ±.20	—
120	1.20 ±.20	1.38 ±.14	1.57 ±.12	1.32 ±.13	—	—
124	1.27 ±.16	1.05 ±.11	1.35 ±.11	1.33 ±.16	—	—
129	1.43 ±.17	1.31 ±.11	1.16 ±.11	1.11 ±.13	1.32 ±.13	—
134	1.17 ±.15	1.01 ±.12	1.61 ±.15	1.28 ±.13	1.62 ±.12	—
138	—	1.00 ±.20	1.30 ±.16	1.62 ±.16	—	--

TABLE Vb

Ne+NaF → π^+ + X

E/A = 655 MeV

$Ed^3\sigma/dp^3$

$\mu b\ c^3/(sr\ MeV^2)$

p_π	θ_π lab. degrees					
MeV/c	24	28	32	36	40	44
146	—	.84 ±.08	.89 ±.08	1.01 ±.09	.95 ±.10	—
151	—	.88 ±.09	1.08 ±.09	.93 ±.09	1.27 ±.11	1.31 ±.11
156	.99 ±.10	.83 ±.08	.98 ±.08	.91 ±.09	1.24 ±.11	1.31 ±.11
161	.76 ±.07	.84 ±.08	1.09 ±.09	.96 ±.09	1.35 ±.11	1.27 ±.11
166	.78 ±.08	.88 ±.06	1.07 ±.09	1.11 ±.10	1.10 ±.11	1.29 ±.10
171	.79 ±.08	.79 ±.05	.91 ±.08	1.06 ±.09	1.44 ±.11	1.45 ±.11
176	.80 ±.07	.76 ±.05	.81 ±.07	1.11 ±.09	1.52 ±.11	1.54 ±.14
181	.57 ±.06	.73 ±.05	.93 ±.06	1.13 ±.09	1.26 ±.11	—
186	.61 ±.06	.70 ±.05	.86 ±.05	1.03 ±.09	1.21 ±.11	—
190	.58 ±.06	.65 ±.05	.91 ±.05	1.04 ±.09	—	—
195	.68 ±.06	.66 ±.04	.88 ±.05	1.10 ±.10	—	—
200	.61 ±.06	.60 ±.04	.88 ±.05	1.10 ±.07	—	—

TABLE VI

$Ar+C \rightarrow \pi^- + X$

E/A = 1.026 GeV

$Ed^3\sigma/dp^3$ $\mu b\ c^3/(sr\ MeV^2)$

p_π MeV/c	θ_π lab. degrees								
	0	4	8	12	16	20	24	28	32
123	4.0 ±.8	4.0 ±.5	5.8 ±.6	4.3 ±.6	4.6 ±.6	—	—	—	—
132	3.7 ±.7	3.7 ±.4	4.5 ±.5	4.6 ±.6	4.2 ±.6	3.9 ±.6	—	—	—
140	3.9 ±.8	4.8 ±.5	4.4 ±.6	4.9 ±.6	4.8 ±.6	3.5 ±.5	4.0 ±.5	—	—
149	4.9 ±.9	5.1 ±.6	4.1 ±.6	4.0 ±.5	4.5 ±.6	4.6 ±.5	3.7 ±.5	—	—
157	—	4.1 ±.7	3.4 ±.5	4.3 ±.6	4.0 ±.5	4.2 ±.5	3.4 ±.4	3.8 ±.4	—
166	—	—	—	3.5 ±.5	4.4 ±.5	4.8 ±.5	3.9 ±.5	4.0 ±.4	3.0 ±.4
175	—	—	—	—	—	3.4 ±.7	3.4 ±.5	3.6 ±.4	2.9 ±.3

TABLE VII

$Ar+Ca \rightarrow \pi^- + X$

E/A = 1.02 GeV

$Ed^3\sigma/dp^3$ $\mu b\ c^3/(sr\ MeV^2)$

p_π MeV/c	θ_π lab. degrees								
	0	4	8	12	16	20	24	28	32
103	11.4 ±1.2	14.6 ±.8	13.8 ±.8	12.5 ±.9	12.8 ±.9	—	—	—	—
109	12.8 ±1.1	15.3 ±.7	14.3 ±.7	13.3 ±.9	14.0 ±.9	13.3 ±.9	—	—	—
116	11.4 ±1.1	15.0 ±.6	13.5 ±.7	15.0 ±.8	14.4 ±.8	12.3 ±.7	12.9 ±.7	—	—
124	13.4 ±1.1	12.7 ±.6	13.6 ±.5	13.5 ±.5	13.1 ±.5	12.8 ±.5	13.3 ±.6	—	—
133	11.9 ±.9	13.7 ±.6	12.5 ±.6	12.0 ±.4	12.7 ±.4	12.1 ±.4	11.5 ±.5	12.1 ±.5	—
141	12.3 ±1.0	12.4 ±.5	12.1 ±.7	12.0 ±.7	11.8 ±.7	10.9 ±.5	9.5 ±.4	10.4 ±.5	9.8 ±.4
149	—	12.3 ±.7	13.5 ±.7	11.9 ±.7	13.4 ±.7	10.6 ±.6	10.9 ±.6	9.9 ±.6	—
158	—	—	12.3 ±.7	11.8 ±.7	11.5 ±.6	11.8 ±.6	10.8 ±.6	11.1 ±.5	—
166	—	—	—	12.0 ±.7	12.6 ±.6	11.3 ±.6	10.9 ±.6	10.5 ±.5	8.7 ±.4
175	—	—	—	—	11.1 ±1.0	11.1 ±.9	11.0 ±.6	9.5 ±.5	8.8 ±.4

TABLE VIII

$Ar+U \rightarrow \pi^- + X$

E/A = 1.026 GeV

$Ed^3\sigma/dp^3$ $\mu b\ c^3/(sr\ MeV^2)$

p_π MeV/c	θ_π lab. degrees								
	0	4	8	12	16	20	24	28	32
100	62.1 ±9.5	92.7 ±6.6	65.7 ±5.8	81.9 ±8.1	81.2 ±7.9	—	—	—	—
106	59.2 ±8.3	82.8 ±5.7	78.3 ±5.8	65.9 ±6.6	88.1 ±7.8	68.6 ±6.8	—	—	—
114	56.7 ±6.2	76.3 ±4.3	67.9 ±5.6	79.3 ±6.4	71.8 ±5.7	70.6 ±5.5	77.1 ±5.9	—	—
122	58.4 ±5.5	69.9 ±3.6	69.5 ±3.0	74.4 ±3.3	65.8 ±3.0	69.6 ±4.3	61.6 ±4.1	—	—
131	69.0 ±5.7	68.5 ±3.3	62.3 ±3.2	62.5 ±2.8	63.4 ±2.8	61.7 ±2.7	52.5 ±3.4	61.4 ±3.6	—
139	52.9 ±5.0	63.1 ±3.1	56.4 ±3.8	57.8 ±3.8	56.7 ±3.8	52.6 ±2.8	45.3 ±2.5	44.7 ±3.6	55.8 ±3.5
148	—	54.5 ±3.8	61.7 ±3.9	51.8 ±3.5	52.3 ±3.5	47.1 ±3.2	51.6 ±3.1	45.5 ±3.4	—
156	—	—	54.2 ±3.6	54.0 ±3.7	52.0 ±3.3	54.5 ±3.3	47.1 ±2.9	52.6 ±3.0	—
165	—	—	—	52.3 ±3.5	51.4 ±3.2	50.0 ±3.0	43.5 ±2.9	45.9 ±2.7	41.5 ±2.5
173	—	—	—	—	47.1 ±5.4	39.7 ±4.2	44.1 ±3.2	38.3 ±2.4	34.6 ±2.0

TABLE IX

$Ar+C \rightarrow \pi^+ + X$

E/A = 1.026 GeV

$Ed^3\sigma/dp^3$ $\mu b\ c^3/(sr\ MeV^2)$

p_π	θ_π lab. degrees								
MeV/c	0	4	8	12	16	20	24	28	32
123	1.7 ±.6	2.7 ±.4	2.6 ±.4	2.3 ±.4	2.7 ±.4	—	—	—	—
132	2.2 ±.5	1.9 ±.3	2.2 ±.3	1.8 ±.4	3.3 ±.4	2.4 ±.4	—	—	—
140	2.7 ±.5	2.9 ±.3	1.8 ±.4	2.7 ±.4	2.5 ±.4	3.0 ±.4	2.0 ±.3	—	—
149	—	3.0 ±.4	3.3 ±.4	2.2 ±.4	2.2 ±.4	1.8 ±.4	1.8 ±.3	—	—
157	—	—	2.5 ±.3	2.3 ±.4	2.4 ±.4	2.8 ±.4	2.6 ±.3	2.5 ±.4	—
166	—	—	1.7 ±.5	2.8 ±.4	2.6 ±.4	2.4 ±.3	3.2 ±.4	2.7 ±.3	2.0 ±.3
175	—	—	—	—	—	2.1 ±.5	2.9 ±.4	2.7 ±.3	1.8 ±.2

TABLE X

$Ar+Ca \rightarrow \pi^+ + X$

E/A = 1.02 GeV

$Ed^3\sigma/dp^3$ $\mu b\ c^3/(sr\ MeV^2)$

p_π	θ_π lab. degrees								
MeV/c	0	4	8	12	16	20	24	28	32
103	8.1 ±1.0	9.0 ±.6	9.6 ±.6	7.6 ±.7	7.6 ±.7	—	—	—	—
109	8.0 ±.9	8.0 ±.5	8.4 ±.5	9.3 ±.7	9.5 ±.7	8.4 ±.7	—	—	—
116	7.3 ±.9	7.5 ±.4	8.6 ±.6	8.8 ±.6	7.9 ±.6	8.5 ±.5	7.8 ±.6	—	—
124	7.6 ±1.1	8.1 ±.6	8.2 ±.4	8.1 ±.4	8.4 ±.4	8.7 ±.4	8.0 ±.4	—	—
133	6.5 ±.9	7.3 ±.6	7.9 ±.6	7.3 ±.3	7.7 ±.3	8.5 ±.4	7.8 ±.4	8.0 ±.4	—
141	6.3 ±.8	8.4 ±.6	8.4 ±.8	8.9 ±.8	8.9 ±.8	7.0 ±.4	7.1 ±.4	6.6 ±.4	8.1 ±.4
149	—	7.3 ±.7	7.8 ±.7	7.7 ±.7	8.0 ±.7	7.1 ±.7	7.7 ±.6	—	—
158	—	—	7.6 ±.7	6.9 ±.7	8.1 ±.7	7.2 ±.6	8.3 ±.6	7.7 ±.6	—
166	—	—	—	7.7 ±.7	7.9 ±.7	8.2 ±.7	8.0 ±.6	7.6 ±.6	6.9 ±.5
175	—	—	—	—	—	8.8 ±1.0	7.8 ±.7	7.4 ±.6	6.4 ±.4

TABLE XI

Ar+U → π^+ + X

E/A = 1.026 GeV

$Ed^3\sigma/dp^3$ μb $c^3/(sr\ MeV^2)$

p_π	θ_π lab. degrees								
MeV/c	0	4	8	12	16	20	24	28	32
100	17.4 ±3.7	23.8 ±2.3	21.6 ±2.2	14.0 ±2.6	18.0 ±2.5	—	—	—	—
106	16.0 ±2.8	23.4 ±2.0	23.8 ±2.1	21.7 ±2.5	24.7 ±2.6	21.9 ±2.5	—	—	—
114	17.0 ±3.0	21.5 ±1.6	20.2 ±2.1	24.3 ±2.5	22.6 ±2.2	22.4 ±2.1	18.0 ±2.0	—	—
122	13.5 ±3.5	21.5 ±2.2	20.8 ±1.4	21.0 ±1.3	22.1 ±1.4	22.8 ±1.6	20.0 ±1.5	23.7 ±1.7	—
131	20.9 ±3.1	20.6 ±2.0	20.5 ±2.1	17.0 ±1.2	19.6 ±1.3	18.4 ±1.2	20.5 ±1.4	21.9 ±1.4	—
139	20.3 ±2.7	24.2 ±1.8	15.2 ±2.3	26.4 ±2.6	17.4 ±2.3	18.9 ±1.5	18.1 ±1.3	20.3 ±1.6	16.0 ±1.3
148	—	20.4 ±2.1	20.0 ±2.2	21.4 ±2.5	22.0 ±2.5	14.4 ±2.2	20.6 ±2.0	—	—
156	—	—	24.3 ±2.2	23.3 ±2.5	18.7 ±2.1	20.0 ±2.3	18.7 ±1.8	17.5 ±2.1	—
165	—	—	—	18.9 ±2.2	20.0 ±2.4	18.3 ±2.1	20.3 ±2.0	18.3 ±1.7	18.9 ±1.7
173	—	—	—	—	—	19.0 ±2.8	15.1 ±2.1	18.7 ±1.8	16.8 ±1.5

LAWRENCE BERKELEY LABORATORY
TECHNICAL INFORMATION DEPARTMENT
UNIVERSITY OF CALIFORNIA
BERKELEY, CALIFORNIA 94720